MUCOSAL IMMUNOLOGY

Airway brush cells generate cysteinyl leukotrienes through the ATP sensor P2Y2

Saltanat Ualiyeva[1], Nils Hallen[1], Yoshihide Kanaoka[1], Carola Ledderose[2], Ichiro Matsumoto[3], Wolfgang G. Junger[2], Nora A. Barrett[1]*, Lora G. Bankova[1]*

Chemosensory epithelial cells (EpCs) are specialized cells that promote innate type 2 immunity and protective neurally mediated reflexes in the airway. Their effector programs and modes of activation are not fully understood. Here, we define the transcriptional signature of two choline acetyltransferase–expressing nasal EpC populations. They are found in the respiratory and olfactory mucosa and express key chemosensory cell genes including the transcription factor *Pou2f3*, the cation channel *Trpm5*, and the cytokine *Il25*. Moreover, these cells share a core transcriptional signature with chemosensory cells from intestine, trachea and thymus, and cluster with tracheal brush cells (BrCs) independently from other respiratory EpCs, indicating that they are part of the brush/tuft cell family. Both nasal BrC subsets express high levels of transcripts encoding cysteinyl leukotriene (CysLT) biosynthetic enzymes. In response to ionophore, unfractionated nasal BrCs generate CysLTs at levels exceeding that of the adjacent hematopoietic cells isolated from naïve mucosa. Among activating receptors, BrCs express the purinergic receptor P2Y2. Accordingly, the epithelial stress signal ATP and aeroallergens that elicit ATP release trigger BrC CysLT generation, which is mediated by the P2Y2 receptor. ATP- and aeroallergen-elicited CysLT generation in the nasal lavage is reduced in mice lacking Pou2f3, a requisite transcription factor for BrC development. Last, aeroallergen-induced airway eosinophilia is reduced in BrC-deficient mice. These results identify a previously undescribed BrC sensor and effector pathway leading to generation of lipid mediators in response to luminal signals. Further, they suggest that BrC sensing of local damage may provide an important sentinel immune function.

INTRODUCTION

Epithelial cells (EpCs) play a critical role in mucosal host defense through a diverse array of innate effector programs. In the airway, they produce interferons and antimicrobial peptides, generate pro-inflammatory cytokines, release mucins, and activate sensory neurons (*1*). Recent work in the human airway at the resolution of a single cell has demonstrated a remarkable subspecialization of these epithelial functions and defined previously undescribed cell types (*2*–*4*), but the pathways connecting EpC recognition of danger to specific effector functions are still poorly defined.

Chemosensory EpCs are detected in the airway, urinary, and gut mucosa (*5*). They are referred to as tuft cells in the intestinal mucosa (*6*–*8*), brush cells (BrCs) in the trachea (*9*), and solitary chemosensory cells (SCCs) in the nasal respiratory mucosa (*10*). They were first characterized by their unique morphology—an amphora or teardrop shape and a "tuft" of short brush-like projections extending into the mucosal lumen (*11*, *12*). Later studies defined some chemosensory cells by their expression of bitter taste receptors and proteins associated with the canonical taste transduction system, including the G protein α-gustducin (*10*, *13*), phospholipase C-β (PLCβ) (*9*, *14*, *15*), and the calcium-activated cation channel transient receptor potential melastatin 5 (TRPM5) (*14*–*17*). These cells are specified by the transcription factor Pou2f3, which is required for their development in the anterior nasal cavity (*18*), the trachea (*19*), and the small intestine (*8*). Microvillus cells (MVCs), a distinct EpC population detected in the mouse olfactory mucosa, express TRPM5 (*20*–*22*) and PLCβ (*23*) and depend on Pou2f3 (*24*). Although MVCs are noted to express taste receptors and *Gnat3* (encoding α-gustducin) at lower levels (*23*), an unsupervised analysis comparing this population with chemosensory EpC subsets has not been reported.

More recent work on this EpC family has elucidated shared functions. For example, chemosensory EpCs are the dominant source of interleukin-25 (IL-25) in the naïve airway and intestinal mucosa. In the intestine, tuft cell IL-25 generation activates IL-13–producing group 2 innate lymphoid cells and elicits goblet cell metaplasia, which is essential for immunity to helminths and parasites (*6*–*8*, *25*, *26*). In the lung, BrC generation of IL-25 promotes eosinophilic type 2 inflammation in response to aeroallergens (*27*). Thus, chemosensory EpCs appear to play an essential upstream role in driving type 2 inflammation elicited by diverse pathogens across mucosal tissues.

In the airways, chemosensory EpCs are noted to have protective functions in some contexts. Tracheal BrCs and SCCs regulate protective respiratory reflexes such as apnea or sneezing in response to activation of canonical taste receptors by bitter compounds, odorants, and bacterial quorum-sensing molecules (*9*, *28*, *29*). This protective function has been most closely linked to their generation of acetylcholine, leading to activation of peptidergic sensory nerve fibers (*9*, *28*). MVCs also generate acetylcholine but use it to modulate the activity of olfactory neurons and maintain homeostasis in the olfactory epithelium (*22*, *30*, *31*). Thus, this second effector pathway endows EpCs with a broader functional capacity to elicit immediate coordinated protective responses at an organismal level.

A common and essential feature of both chemosensory EpCs and MVCs is their ability to rapidly respond to relevant luminal stimuli with changes in intracellular calcium levels (*14*, *17*, *22*), a flux required for TRPM5 activation (*32*) and subsequent acetylcholine release (*33*). Calcium flux is also essential for the generation of eicosanoids such

[1]Division of Allergy and Clinical Immunology, Jeff and Penny Vinik Center for Allergic Disease Research, Brigham and Women's Hospital and Department of Medicine, Harvard Medical School, Boston, MA, USA. [2]Department of Surgery, Beth Israel Deaconess Medical Center, Harvard Medical School, Boston, MA, USA. [3]Monell Chemical Senses Center, Philadelphia, PA, USA.
*Corresponding author. Email: lbankova@bwh.harvard.edu (L.G.B.); nbarrett@bwh.harvard.edu (N.A.B.)

as cysteinyl leukotrienes (CysLTs). These potent proinflammatory lipids have been implicated as possible chemosensory EpC mediators based on the detection of high levels of transcripts encoding CysLT biosynthetic enzymes in intestinal tuft cells (*15*, *25*, *34*) and tracheal BrCs (*2*, *3*, *27*). Furthermore, we recently reported that CysLT generation in the respiratory tract occurs in concert with BrC activation (*27*), but whether BrCs actually generate CysLTs and the mechanism by which that may occur has not been explored.

CysLTs (leukotriene C4, LTD_4, and LTE_4) are derived from arachidonic acid through the 5-lipoxygenase (5-LO) pathway. On cell activation, group IV cytosolic phospholipase A2 (cPLA2α) cleaves phospholipids at the outer nuclear membrane to generate free arachidonate. 5-LO then oxidizes arachidonic acid in the presence of 5-LO–activating protein (FLAP) to generate leukotriene A_4 (LTA_4), which is subsequently converted to LTC_4 by leukotriene C_4 synthase (LTC_4S) (*35*). After export from the cell, LTC_4 is converted to LTD_4 and LTE_4 by γ-glutamyl transpeptidases and dipeptidases (*36*). Both cPLA2α and 5-LO require calcium for translocation to the nuclear membrane (*37*, *38*). Accordingly, Syk-dependent leukocyte receptors that elicit sustained fluxes in intracellular calcium such as FcεR1 (*39*, *40*) and the fungal receptors Dectin-1 (*41*) and Dectin-2 (*42*) elicit robust generation of CysLTs, whereas Toll-like receptor signaling does not (*43*).

Although no EpC receptors are reported to mediate CysLT generation, we previously found that airway inhalation of the fungal species *Alternaria alternata* (*Alternaria*) elicits important CysLT-dependent epithelial defenses including the rapid release of goblet cell mucin in the nasal mucosa over minutes (*44*) and the expansion of IL-25–producing BrCs in the trachea over days (*27*). Thus, we hypothesized that airway BrCs may generate high quantities of CysLTs and that we might use this function to further define the molecular signaling regulating BrC sensing.

Here, we establish flow cytometric criteria to preferentially enrich for choline acetyltransferase–positive ($ChAT^+$) MVCs or $ChAT^+$ SCCs in the nasal mucosa and perform transcriptional profiling to understand their sensing capacity and effector programs. As expected, each population expresses *Pou2f3* and *Trpm5*. These nasal MVCs and SCCs are enriched for 64 or 63 of the 88 genes previously reported to be the transcriptional signature of brush/tuft cells (*25*), and each population clusters with tracheal BrCs independently from other airway EpCs, indicating that they are in the BrC family. We find that CysLT-generating enzymes are among the most highly expressed transcripts that distinguish these airway BrC subsets from surrounding EpCs. Ex vivo stimulation of unfractionated nasal BrCs with calcium ionophore elicits robust generation of CysLTs that exceed the levels generated by adjacent $CD45^+$ leukocytes. Furthermore, we find that the damage-associated molecules adenosine triphosphate (ATP) and uridine triphosphate (UTP) and complex aeroallergens, including the house dust mite *Dermatophagoides pteronyssinus* (*Dp*) and the mold *Alternaria*, elicit robust BrC generation of CysLTs. Inhibition of the nucleotide receptor P2Y2 and genetic deletion in $P2ry2^{-/-}$ mice abolished CysLT generation elicited by ATP. P2Y2 receptor inhibition also significantly reduced *Alternaria*-elicited CysLTs, establishing P2Y2 as a previously unrecognized BrC receptor involved in sensing a common environmental microbe. CysLT generation was absent in the nasal lavage of ATP-challenged $P2ry2^{-/-}$ mice and ATP- or aeroallergen-challenged $Pou2f3^{-/-}$ BrC-deficient mice, demonstrating that this previously undescribed BrC effector pathway can be elicited by aeroallergens and damage-associated molecular patterns in the airway. Last, *Alternaria*-triggered airway eosinophilia at early and later time points was selectively reduced in BrC-deficient $Pou2f3^{-/-}$ mice, demonstrating the importance of BrCs in previously established models of innate and adaptive type 2 inflammation.

RESULTS

Two populations of nasal ChAT-eGFP$^+$ EpCs share the BrC signature

To define the shared and unique features of ChAT–enhanced green fluorescent protein–positive ($eGFP^+$) EpCs in the upper and lower airways, we first isolated ChAT-$eGFP^+$ EpCs from the nasal mucosa of naïve $ChAT^{(BAC)}$-eGFP mice (*45*) and compared them with tracheal BrCs from our previous study (*27*). Nasal ChAT-$eGFP^+$ EpCs were similar to tracheal BrCs in their expression of high levels of epithelial cell adhesion molecule (EpCAM) and ChAT-eGFP. However, in the nose, the ChAT-$eGFP^+$ EpCs accounted for a much higher portion of $EpCAM^+$ EpCs, at 4 to 5% of live $CD45^{low/-}$ cells and 2 to 3% of all live cells (Fig. 1, A and B), compared with 0.5% as reported in the lower airways (*9*, *27*) and intestine (*6*, *7*, *25*). Thus, >18,000 ChAT-$eGFP^+$ EpCs could be recovered per mouse nose. Fluorescence-activated cell sorting (FACS) analysis of nasal ChAT-$eGFP^+$ BrCs demonstrated a distinct profile. Only a small portion of ChAT-$eGFP^+$ EpCs in the nose had high forward scatter (FSC) and high side scatter (SSC) characteristics similar to tracheal BrCs (fig. S1A) (*27*). These $FSC^{hi}SSC^{hi}$ cells accounted for 5% of ChAT-$eGFP^+$ EpCs in the nose. Most (95%) of the nasal ChAT-$eGFP^+$ EpCs were FSC low and SSC low, suggesting that they are smaller and agranular. ChAT-$eGFP^+$ EpCs have been previously reported in two locations in the nasal mucosa. In the respiratory mucosa and vomeronasal organ, ChAT-expressing EpCs are rare, large, and morphologically complex cells with processes extending to both the luminal surface and basal side of the epithelium and are referred to as SCCs (*28*, *46*). By contrast, in the olfactory mucosa, ChAT-$eGFP^+$ EpCs are smaller, are more abundant, have a more uniform structure, and are termed MVCs (*22*). Thus, their relative frequency and flow cytometric parameters suggest that the $FSC^{hi}SSC^{hi}$ ChAT-$eGFP^+$ EpCs may be classical SCCs, which derive from the respiratory mucosa, whereas the $FSC^{low}SSC^{low}$ ChAT-$eGFP^+$ EpCs may be MVCs, which derive from the olfactory mucosa.

To more clearly define these populations, we sorted each separately and compared them with tracheal ChAT-$eGFP^+$ BrCs from our previously published RNA sequencing analysis (*27*). Like tracheal BrCs (also ChAT-$eGFP^+$), both populations of nasal ChAT-$eGFP^+$ cells express high levels of *Chat*, encoding ChAT; *Pou2f3*, the transcription factor required for the development of chemosensory cells in the airway and intestine (*8*, *18*, *19*, *24*); and *Trpm5*, encoding the calcium-activated, nonselective cation channel TRPM5 specific to taste-transducing cells (*47*). Other BrC-specific markers (*Plcb2*, *Avil*, and *Sox9*) were also expressed in all airway ChAT-$eGFP^+$ cells (Fig. 1C). To further define the possible functional heterogeneity between the three populations of airway ChAT-$eGFP^+$ EpCs, we performed hierarchical clustering of the 50 most highly variable genes among nasal and tracheal ChAT-$eGFP^+$ EpCs (Fig. 1D). This analysis suggested that tracheal BrCs were more similar to $FSC^{hi}SSC^{hi}$ ChAT-$eGFP^+$ EpCs than to $FSC^{low}SSC^{low}$ ChAT-$eGFP^+$ EpCs. Canonical taste receptors were more highly expressed in $FSC^{hi}SSC^{hi}$ ChAT-$eGFP^+$ cells and tracheal BrCs than in $FSC^{low}SSC^{low}$ ChAT-$eGFP^+$ cells, but some were expressed in all subsets (Fig. 1D and fig. S1B). On the other hand, the transcripts for the chemosensory cell–specific cytokine

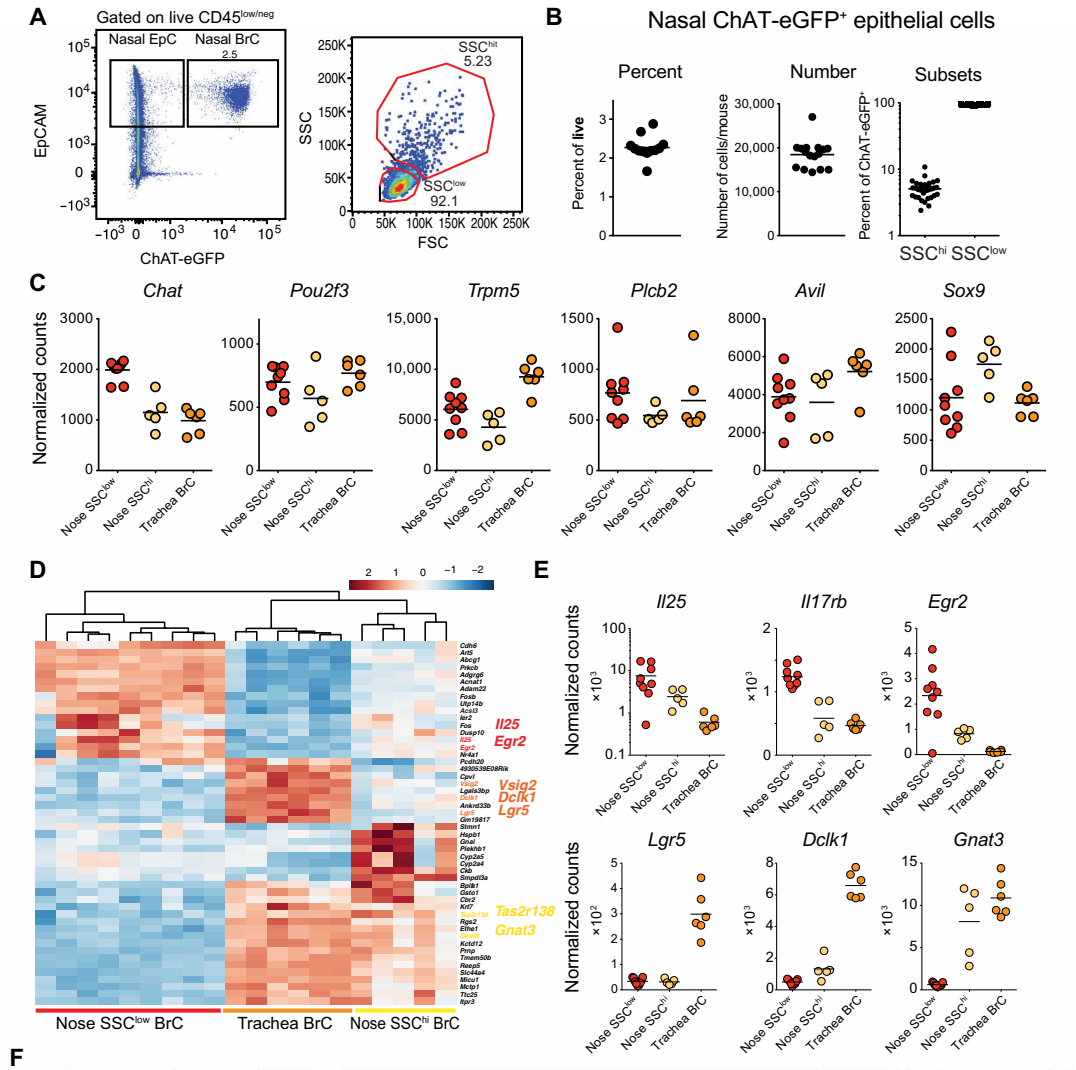

Fig. 1. Two populations of nasal ChAT-eGFP$^+$ EpCs belong to the BrC/tuft cell family. (**A** to **D**) EpCAM$^+$ CD45$^{-/low}$eGFP$^+$ and EpCAM$^+$CD45$^{-/low}$ eGFP$^-$ EpCs were isolated by FACS sorting from naïve nasal mucosa of ChAT-eGFP mice. (A) FACS gating strategy demonstrating two populations of nasal ChAT-eGFP$^+$ EpCs. (B) ChAT-eGFP$^+$ EpCs recovered as a percent of all live cells (left) and the total number recovered per mouse (middle). Frequency of FSC^{hi}SSC^{hi} and FSC^{low}SSC^{low} ChAT-eGFP$^+$ EpCs as a percent of all ChAT-eGFP$^+$ EpCs (right). (C and **E**). Normalized counts of the indicated genes derived from RNA sequencing analysis using DeSeq2. (D) Hierarchical clustering of the top 50 most variably expressed genes among the ChAT-eGFP$^+$ EpCs in the trachea and nose. (**F**) Whole mount of nasal septum of a ChAT-eGFP mouse, eGFP fluorescence was enhanced with an anti-eGFP antibody (green). (**G**) Whole nasal septum staining for DCLK1 (red), ChAT-eGFP (green), and EpCAM (gray). (**H**) Cross section of the nasal cavity and staining of paraffin-embedded slides for ChAT-eGFP (green), Gα-gustducin (red), and Hoechst (blue).

IL-25 and its receptor IL-17RB were more highly expressed in FSC^{low}SSC^{low} ChAT-eGFP$^+$ cells (Fig. 1, D and E), suggesting differential capacity to respond to the environment. FSC^{low}SSC^{low} ChAT-eGFP$^+$ EpCs differentially expressed the zinc factor transcription factor *Egr2* involved in both immune and peripheral nervous cell maturation (*48*–*50*). Last, in contrast to tracheal BrCs, both FSC^{low}SSC^{low} and FSC^{hi}SSC^{hi} ChAT-eGFP$^+$ nasal EpCs express low levels of the Wnt pathway–associated stem cell G protein–coupled receptor (GPCR) *Lgr5* (*51*), suggesting that some of the genes marking these populations are specific to their location in the upper versus lower airways. The chemosensory cell markers *Gnat3*, encoding the taste transduction

protein Gα-gustducin, and *Dclk1*, encoding the chemosensory cell–specific cytoskeletal protein doublecortin like kinase 1 (DCLK1), were expressed in tracheal BrCs and $FSC^{hi}FSC^{hi}$ ChAT-eGFP$^+$ EpCs at much higher levels than in $FSC^{low}SSC^{low}$ ChAT-eGFP$^+$ EpCs (Fig. 1E). We also compared the two nasal ChAT-eGFP$^+$ EpC populations with the shared brush/tuft cell signature of intestinal, tracheal, thymus, and gallbladder tuft cells (*25*). $FSC^{low}SSC^{low}$ ChAT-eGFP$^+$ EpCs demonstrated twofold enrichment for 64 of the 88 genes identified as a pan-tuft cell signature, whereas $FSC^{hi}SSC^{hi}$ ChAT-eGFP$^+$ EpCs demonstrated twofold enrichment for 63 of the 88 genes identified as pan-tuft cell signature (fig. S1C) (*25*), indicating that both nasal ChAT-eGFP$^+$ EpC populations were in the BrC/tuft cell family.

To confirm that our sorted $FSC^{low}SSC^{low}$ and $FSC^{hi}SSC^{hi}$ ChAT-eGFP$^+$ EpCs represented the previously reported olfactory mucosal MVCs and respiratory mucosal SCCs, respectively, we assessed them in situ. As expected, ChAT-eGFP$^+$ BrCs were rare in the nasal respiratory epithelium and highly concentrated in the main olfactory epithelium (Fig. 1F). Cells found in the two locations varied in size and morphology, with smaller uniform cells in the olfactory epithelium and larger morphologically heterogeneous BrCs in the respiratory epithelium, consistent with the numbers and FSC and SSC characteristics of our $FSC^{low}SSC^{low}$ and $FSC^{hi}FSC^{hi}$ ChAT-eGFP$^+$ EpCs, respectively. To validate these assignments, we assessed DCLK1 and Gα-gustducin, each of which was expressed at higher levels in the transcriptome of $FSC^{hi}SSC^{hi}$ ChAT-eGFP$^+$ EpCs, compared with $FSC^{low}SSC^{low}$ ChAT-eGFP$^+$ EpCs. Although ChAT-eGFP$^+$ EpCs in the respiratory mucosa expressed DCLK1 (Fig. 1G) and Gα-gustducin (Fig. 1H), we did not detect either marker by histology in the ChAT-eGFP$^+$ EpCs in the olfactory epithelium, consistent with previous reports (*10*, *21*, *24*, *52*). This suggests that the rare, large $FSC^{hi}SSC^{hi}$ ChAT-eGFP$^+$ EpCs, expressing *Dclk1* and *Gnat3*, correspond to the BrCs in the respiratory epithelium, whereas the abundant, small $FSC^{low}SSC^{low}$ ChAT-eGFP$^+$ EpCs correspond to the homogeneous smaller, DCLK1- and Gα-gustducin–negative BrCs in the olfactory epithelium. Hereafter, we refer to them as respiratory and olfactory BrCs.

Thus, together, we find that two subsets of nasal ChAT-eGFP$^+$ EpCs are unique but share a large number of genes with chemosensory EpCs in the trachea, intestine, gallbladder, and thymus (*25*, *27*). Both ChAT-expressing EpC subsets are part of the BrC/tuft cell family. Nasal respiratory and olfactory BrCs (corresponding to SCCs and MVCs, respectively) express both IL-25 and ChAT, indicating that they are each poised to generate diverse effector molecules and elicit both immune and neural effector functions. Furthermore, we find that ChAT-eGFP$^+$ EpCs are sufficiently abundant in the naïve nasal mucosa of mice to allow for isolation and ex vivo functional experiments.

Nasal BrCs are the dominant source of CysLTs in the naïve nasal airway mucosa

To define the unique functions of airway BrCs, we next compared the transcriptional profile of nasal and tracheal $EpCAM^+eGFP^+$ BrCs with nasal and tracheal $EpCAM^+eGFP^-$ EpCs. Principal components analysis demonstrated that the three populations of airway BrCs were grouped not only quite distinctly from other EpCs but also separately from each other (Fig. 2A). The degree of similarity between tracheal BrCs and the two subsets of nasal BrCs was further highlighted by their closeness when we performed Euclidean distance measurements. This analysis demonstrates that the three subsets of BrCs are distinct but notably closer to each other than to either nasal or tracheal EpCs (Fig. 2B). To determine the features that distinguish airway BrCs from the rest of airway EpCs, we evaluated the 100 most highly variable genes, defining a core signature shared between tracheal, nasal respiratory, and nasal olfactory BrCs (Fig. 2C). As expected, among the shared genes were the pan-tuft cell marker villin (*Avil*), the tuft cell–specific cytokine *Il25*, and the taste transduction machinery genes *Trpm5* and *Gnat3*, as well as the bitter taste receptor *Tas2r108*. The nasal EpCs were a mixture of cell types as evidenced by their high differential expression of genes in the ciliated, goblet, club, and basal airway epithelial signature defined by single-cell sequencing of mouse tracheas (fig. S2A) (*2*). Among the most highly differentially expressed genes conserved across all BrCs were transcripts encoding three proteins critical to CysLT biosynthesis—*Alox5ap* (5-LO activating protein, FLAP), *Alox5* (5-LO), and *Ltc4s* (LTC_4S) (Fig. 2C and fig. S2B). In addition, BrCs had conserved expression of genes linked to calcium signaling in the phosphatidylinositol-phospholipase signaling pathway. Among them were *Pik3r5*, encoding the regulatory subunit of phosphatidylinositol 3-kinase, and *Pik3cg*, encoding phosphatidylinositol-4,5-bisphosphate 3-kinase catalytic subunit gamma. Additional signaling proteins that were highly expressed in airway BrCs included the genes related to chemosensory signaling *Plcb2*, *Plcg2*, and *Itpr2* (fig. S2C). The transcripts *Alox5*, *Alox5ap*, and *Ltc4s*, as well as *Pla2g4a* (cPLA2α), were expressed at remarkably high levels in all airway BrCs (Fig. 2D). BrCs also expressed *Abcc1*, encoding multidrug resistance–associated transporter 1 that allows for LTC_4 export to the extracellular space, where it can be rapidly converted to LTD_4 and LTE_4 (*36*). In contrast, *Lta4h* encoding the enzyme that converts LTA_4 to LTB_4 was not differentially expressed in BrCs. Collectively, these data suggest that airway BrCs are poised to respond to luminal signals with a robust calcium signaling and CysLT generation.

CysLT generation is best characterized in myeloid cells including mast cells, macrophages, and dendritic cells (*40*, *42*). To confirm that CysLTs are generated by BrCs at appreciable levels, we developed an ex vivo protocol for BrC stimulation. Olfactory and respiratory nasal BrCs were not distinguished in these experiments because each population expresses high levels of CysLT-generating enzymes and the respiratory BrCs are less abundant. We isolated nasal BrCs, rested them for 18 hours, stimulated them with calcium ionophore A23187, and compared their CysLT-generating capacity with that of sorted $CD45^+$ hematopoietic cells and ChAT-eGFP$^-$ EpCs in the nasal mucosa. Isolated nasal BrCs stimulated with calcium ionophore generated high levels of CysLTs (Fig. 2E). MK-886, an inhibitor of FLAP, reduced CysLT generation, indicating activity of the conventional CysLT biosynthetic pathway. Although ChAT-eGFP$^-$ nasal EpCs did not generate any appreciable levels of CysLTs (Fig. 2E), $CD45^+$ hematopoietic cells isolated from the nasal mucosa of the same mice generated CysLTs, as expected (Fig. 2E). The pool included $CD11c^+MHC^+$ dendritic cells and $CD11b^+CD11c^+SiglecF^+$ monocytes/macrophages (fig. S3A). Among the other populations known to produce CysLTs, $CD11b^+CD11c^-SiglecF^+$ eosinophils (fig. S3A) and $FcεR1^+CD117^+$ mast cells (fig. S3B) were extremely rare in the digested naïve nasal mucosa, consistent with our previous extensive histologic evaluation (*44*). Unexpectedly, on a per-cell basis, BrC CysLT generation exceeded the level elicited from $CD45^+$ cells even when normalized for cell count. Thus, although 10% of the $CD45^+$ cell group was dendritic cells, the level of CysLTs generated

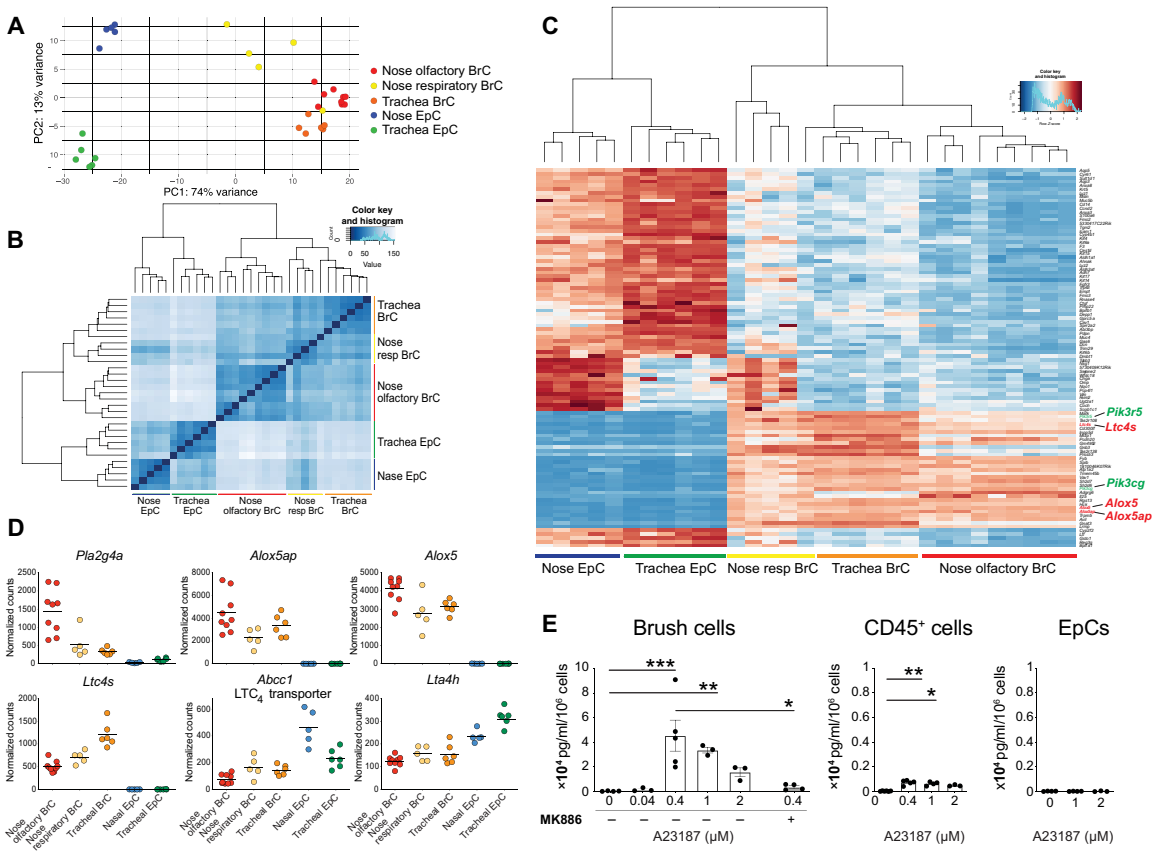

Fig. 2. Airway BrCs are potent producers of CysLTs. (**A**) Principal components analysis of ChAT-eGFP$^+$ BrCs and ChAT-eGFP$^-$ EpCs from the nose and trachea using the top 100 most variable transcripts. Numbers indicate frequency of transcripts described by each principal component (PC). (**B**) Euclidean distance matrix of the rlog-transformed values derived from RNA sequencing. (**C**) Hierarchical clustering of the top 100 most variable genes derived from DeSeq2 analysis. Transcripts of enzymes in the CysLT biosynthetic pathway are highlighted in red. Transcripts of proteins in the phosphatidylinositol pathway are highlighted in green. (**D**) Normalized counts of transcripts encoding CysLT biosynthetic enzymes and transporters. (**E**) BrCs (EpCAM$^+$CD45$^{low/-}$eGFP$^+$), CD45$^+$ cells, and EpCs (EpCAM$^+$CD45$^-$eGFP$^-$) were isolated from the nasal mucosa and stimulated ex vivo with the indicated doses of calcium ionophore (A23187). Where indicated, cells were pretreated for 15 min with the FLAP inhibitor MK-886. The concentration of CysLTs in the supernatants was measured by ELISA at 30 min. Data are means ± SEM from at least three independent experiments, each dot represents a separate biological replicate, *P < 0.05, **P < 0.01, ***P < 0.001.

from the CD45$^+$ pool was less than 10% of that generated by BrCs. To consider the potential contribution of BrCs to the total CysLT-generating capacity of the naïve nasal mucosa, we multiplied the CysLTs generated on a per-cell basis by the number of cells recovered per mouse. Nasal BrCs accounted for >80% of the total CysLT-generating capacity of the naïve nasal mucosa (fig. S3C), suggesting that this cell type is a significant source of CysLTs. Collectively, our data indicate that a core feature of airway BrCs is their ability to respond to activating stimuli with robust CysLT generation.

P2Y2 receptor activation elicits BrC generation of CysLTs

Having established a biologically relevant ex vivo assay for BrC function, we sought to identify the receptors that may trigger CysLT generation. We first focused on GPCRs, some of which are highly expressed in chemosensory EpCs and elicit calcium flux by coupling to Gq. Because olfactory BrCs account for >95% of BrCs in the nose and likely contribute to the bulk of CysLT production, we performed a pairwise comparison between olfactory BrCs and nasal EpCs across 632 GPCRs from the GPCR databank (https://gpcrdb.org). Several taste receptor genes—including *Tas1r3*, *Tas2r126*, *Tas2r108*, and *Tas2r138*—were more highly expressed in respiratory and olfactory BrCs as compared with noncholinergic airway EpC (Fig. 3A and fig. S4, A and B). Consistent with their closer relationship to tracheal BrCs, respiratory BrCs expressed a wider array of taste receptor transcripts at high levels (fig. S4B). The transcript for the succinate receptor *Sucnr1*, an activating receptor on intestinal chemosensory tuft cells (*25*, *26*, *53*), was expressed in tracheal BrCs at much higher levels than in nasal respiratory BrCs and was undetectable in nasal olfactory BrCs (fig. S4C). Among the differentially expressed transcripts in olfactory BrCs was *P2ry2*, the gene encoding the Gq-coupled receptor P2Y2 (Fig. 3A). Further assessment of the purinergic receptor family demonstrated that P2Y2 and P2X4 receptors were highly expressed in all three airway BrC populations, whereas the rest of the purinergic receptors were expressed at low or undetectable levels (Fig. 3B). Together, these results highlight the heterogeneity of activating receptors expressed by chemosensory EpCs that might reflect the local requirement for innate responses to pathogens, allergens, and metabolites.

The purinergic receptors have both overlapping and distinct affinities for the nucleotides ATP, ADP (adenosine diphosphate), and UTP (*54*–*58*). Both ATP and UTP are recognized by P2Y2 receptor, whereas the P2X4 receptor is selectively activated by ATP (*59*). To determine whether the purinergic ligand ATP activates BrCs to produce CysLTs, we first stimulated BrCs isolated from ChAT-eGFP mice with increasing concentrations of ATP and measured CysLTs in the supernatant. The stable analog ATPγS elicited CysLTs from BrCs in a dose-dependent fashion that was detected at 100 μM and peaked at 500 μM (Fig. 3C). The dose response and peak quantity of CysLT generation were similar to that of ATPγS-stimulated bone marrow–derived mast cells (BMMCs) (Fig. 3D),

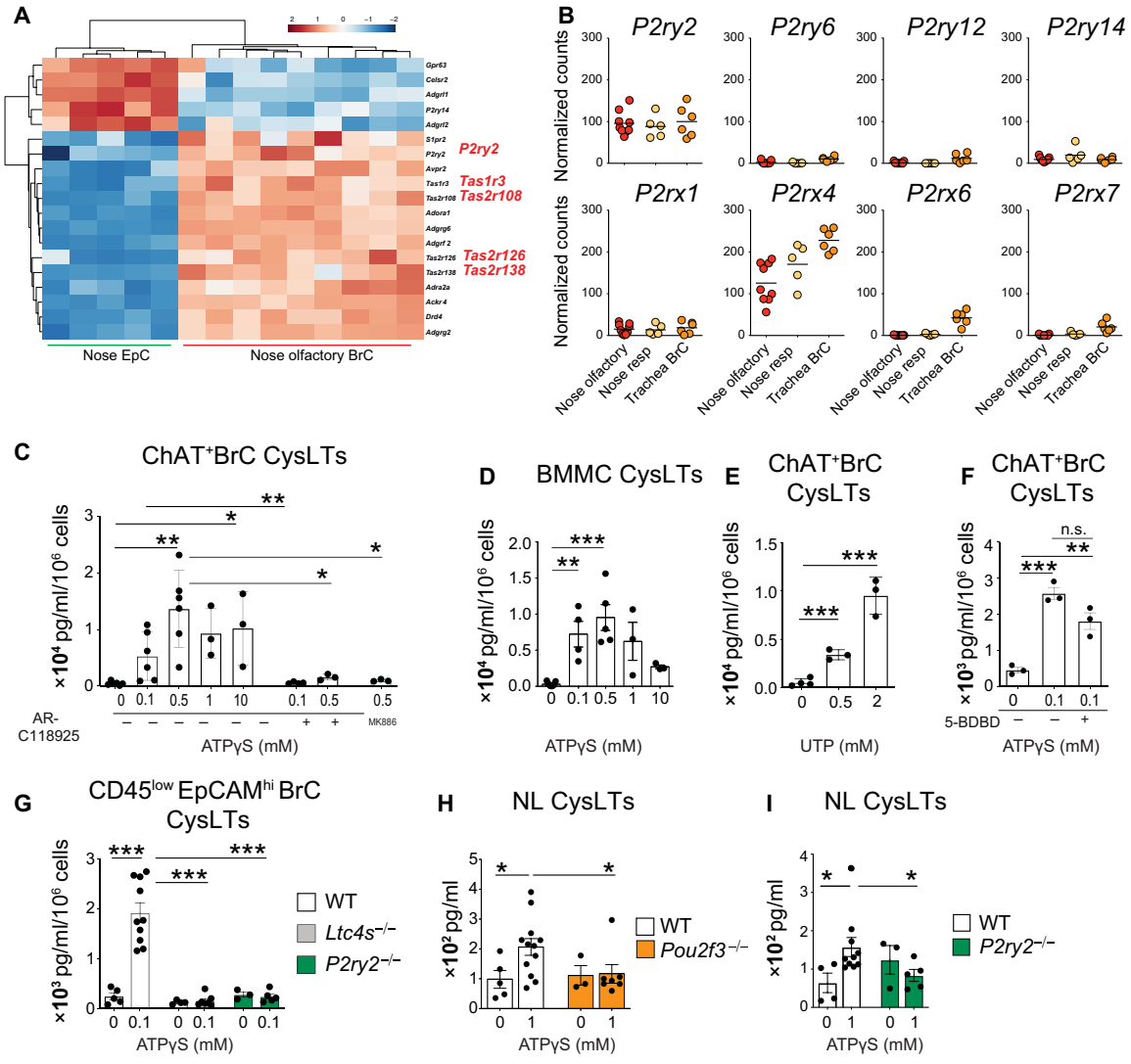

Fig. 3. P2Y2 receptor activation elicits CysLTs from airway BrCs. (**A**) Transcripts of differentially expressed GPCRs in olfactory nasal BrCs compared with nasal EpCs using criteria of $\log_2$ fold change of 2 or greater expression in one relative to the other with a *P* adjusted value of <0.01. (**B**) Transcripts for genes encoding purinergic receptors expressed at levels of 5 or above among nasal BrCs. (**C** and **E**) BrCs (EpCAM$^+$ CD45$^{low/-}$eGFP$^+$) were isolated from the nasal mucosa (nose) of ChAT-eGFP mice and were stimulated ex vivo with the indicated doses of ATPγS (C) or UTP (E) for 30 min. Where indicated, BrCs were pretreated for 15 min with the P2RY2-specific inhibitor AR-C118925, the FLAP inhibitor MK-886, or HBSS and subsequently stimulated with ATPγS. (**D**) Mouse BMMCs were stimulated with ATPγS for 30 min. The concentrations of CysLTs in the supernatants were measured by ELISA at 30 min. (**F**) ChAT-eGFP$^+$ BrCs were pretreated for 15 min with the P2X4-specific inhibitor 5-BDBD and subsequently stimulated with ATPγS. CysLTs were measured in the supernatant at 30 min. (**G**) CD45^{low}EpCAM^{hi} BrCs from WT, *Ltc4s*$^{-/-}$, and *P2ry2*$^{-/-}$ mice were stimulated ex vivo with 0.1 mM ATPγS. The concentration of CysLTs was measured by ELISA. (**H** and **I**) ATP at the indicated dose was administered intranasally to naïve WT, *Pou2f3*$^{-/-}$ (H), and *P2ry2*$^{-/-}$ (I) mice, and nasal lavage (NL) was obtained at 30 min. The concentration of CysLTs was measured by ELISA after acetone precipitation. Data are means ± SEM, each dot is a separate biological replicate, data are pooled from at least two independent experiments **P* < 0.05, ***P* < 0.01, ****P* < 0.001. n.s., not significant.

which express several purinergic receptors (*60*, *61*). CysLT generation was blunted in cells treated with the FLAP inhibitor MK-886, confirming the specificity of the assay (Fig. 3C). BrC viability both an hour after sorting and after overnight rest was preserved, as demonstrated by minimal lactate dehydrogenase (LDH) release (fig. S4D). Consistent with that, ATP-mediated CysLT generation was not different in paired samples of BrCs stimulated with ATPγS at 3 and 18 hours after isolation (fig. S4E).

Pretreatment of BrCs with the P2Y2 receptor inhibitor AR-C118925 also significantly reduced BrC CysLTs elicited by both 100 and 500 μM ATPγS (Fig. 3C), suggesting that P2Y2 is a BrC receptor mediating ATP-elicited generation of CysLTs. Accordingly, UTP stimulation of BrCs also triggered CysLT generation (Fig. 3E) and was inhibited by AR-C118925 (fig. S4F). Whereas no ATPγS-elicited CysLT generation was detected in the presence of the P2Y2 receptor inhibitor AR-C118925 (Fig. 3C), there was significant induction of CysLT generation in the presence of the P2X4 receptor inhibitor 5-(3-bromophenyl)-1,3-dihydro-2*H*-benzofuro[3,2-*e*]-1,4-diazepin-2-one (5-BDBD) (Fig. 3F) (*62*). Together, our pharmacologic studies strongly suggested that ATP is a potent signal for BrC activation for CysLT generation through the P2Y2 receptor.

To confirm the importance of P2Y2 receptor signaling in mice with genetic deletion of P2Y2, we first sought to identify BrCs in the naïve nasal mucosa of wild-type (WT) mice without fluorescent reporter expression. Two recent studies (*2*, *34*) have noted that both intestinal tuft and tracheal BrCs express appreciable levels of *Ptprc*, the transcript encoding the hematopoietic receptor CD45. We found that *Ptprc* was also expressed in nasal BrCs (fig. S5A) and confirmed that low levels of CD45 are expressed in nasal ChAT-eGFP$^+$ EpCs by FACS (fig. S5B). Backgating on CD45^{low}EpCAM^{hi} cells in

ChAT-eGFP mice showed that this population was greatly enriched for BrCs, as 90% percent of this population was ChAT-eGPF$^+$ (fig. S5C). However, this cell isolation strategy was not sensitive to capture all ChAT-eGFP$^+$ cells, given the low CD45 median fluorescence intensity, only two logs higher than the negative population. When compared with WT mice, the CD45^{low}EpCAM^{hi} cells were nearly absent in *Pou2f3*$^{-/-}$ mice, confirming that CD45^{low}EpCAM^{hi} cells are dominantly BrCs (fig. S5D). Pooled CD45$^+$ cells and pooled EpCAM$^+$ EpC numbers were unchanged in the *Pou2f3*$^{-/-}$ mice (fig. S5E). We confirmed that these CD45^{low}EpCAM^{hi} cells isolated from WT mice generate CysLTs in response to stimulation with ATP (fig. S5F). When compared with CD45$^-$EpCAM^{hi} cells, CD45^{low}EpCAM^{hi} cells generated higher levels of CysLTs on a per-cell basis (fig. S5F). The detection of CysLTs in the supernatants of CD45$^-$EpCAM^{hi} EpCs, a population of mixed CD45$^-$BrCs and EpCs, suggests that both BrCs with higher and lower expression of CD45 are capable of generating CysLTs. We isolated CD45^{low}EpCAM^{hi} BrCs from WT, *Ltc4s*$^{-/-}$, and *P2ry2*$^{-/-}$ mice and measured the levels of CysLTs in the supernatant after ex vivo ATPγS stimulation. CysLTs were detectable in the supernatants of ATPγS-stimulated CD45^{low}EpCAM^{hi} BrCs from WT mice but were absent in those isolated from *Ltc4s*$^{-/-}$ mice, confirming that CysLTs generated in response to ATPγS are a product of the classical CysLT biosynthetic cascade (Fig. 3G). CysLT generation was absent in the supernatants of CD45^{low}EpCAM^{hi} BrCs isolated from *P2ry2*$^{-/-}$ mice (Fig. 3G) defining P2Y2 as the specific BrC receptor triggered by ATP for CysLT generation.

To determine whether this alarmin recognition system that we characterized on isolated BrCs was operative in vivo, we instilled ATPγS intranasally and measured CysLTs in the acetone-precipitated nasal lavage 30 min later. ATP elicited dose-dependent CysLT generation in naïve WT mice (fig. S4G). By contrast, there was no response to intranasal ATP in BrC-deficient *Pou2f3*$^{-/-}$ mice (Fig. 3H) or in mice lacking the P2Y2 receptor (Fig. 3I), indicating that airway BrCs respond to the alarmin ATP with robust generation of CysLTs in the nasal mucosa mediated through the P2Y2 receptor.

Aeroallergens elicit P2Y2-dependent BrC CysLT generation and BrC-dependent airway eosinophilia

Several common airborne aeroallergens have been reported to trigger the calcium-dependent exocytosis of ATP from human airway EpCs (*63*, *64*). To determine whether aeroallergens trigger BrC CysLT generation and whether it may be mediated by P2Y2, we incubated BrCs ex vivo with increasing doses of the mold aeroallergen *Alternaria* or the house dust mite aeroallergen *Dp*. Both *Alternaria* and *Dp* elicited CysLTs from BrCs at doses of 400 and 800 μg/ml (Fig. 4A). CysLT generation from *Alternaria*- or *Dp*-stimulated CD45$^+$ cells and *Alternaria*- stimulated EpCs isolated from the same mice was negligible (Fig. 4, B and C). Consistent with that, CysLTs were absent in the supernatants of *Alternaria*-stimulated CD45^{low}EpCAM^{hi} BrCs isolated from *Ltc4s*$^{-/-}$ mice (Fig. 4D), confirming the specificity of CysLT generation in response to this complex allergen extract. Pretreatment of BrCs with the P2Y2 receptor inhibitor AR-C118925 significantly reduced *Alternaria*-elicited CysLTs in the supernatant (Fig. 4E). Thus, although ATP is a direct activator of P2Y2 (*58*), allergens such as *Alternaria* and *Dp* elicit CysLTs, in part, through the indirect release of ATP from BrCs (*63*). These results demonstrate that P2Y2 receptor-mediated CysLT generation is a BrC effector pathway relevant to airborne exposures.

To test the importance of this system in an integrated model, we challenged naïve mice with *Alternaria* intranasally and measured CysLTs in acetone-precipitated nasal lavage. *Alternaria*-elicited CysLT generation was detected in the lavage from WT mice but was significantly reduced in that from BrC-deficient *Pou2f3*$^{-/-}$ mice (Fig. 4F). These results define BrCs as a major source of immunoglobulin E (IgE)–independent airway CysLT generation triggered by aeroallergens (fig. S6). Together, we identify CysLT generation as a third distinct BrC effector function and P2Y2 as a previously undescribed BrC sensor. Furthermore, our findings demonstrate a sentinel role for BrCs in immune recognition of aeroallergens and suggest that they play a likely role in recognition of additional luminal danger signals that elicit tissue damage.

Last, to assess the potential importance of BrCs in airway inflammation, we evaluated the recruitment of inflammatory cells in the bronchoalveolar lavage (BAL) in two previously established models of *Alternaria*-elicited lung inflammation that rely on either innate immune pathways at 24 hours after a single inhalation or a mix of innate and adaptive pathways triggered by repetitive inhalation (*27*, *65*–*67*). As expected, WT mice developed BAL eosinophilia 24 hours after a single *Alternaria* challenge, and eosinophilia increased after four challenges over 9 days (Fig. 4G). BrC-deficient *Pou2f3*$^{-/-}$ mice had reduced BAL eosinophilia at each time point but no reduction in neutrophilia or mononuclear cell infiltrate, pointing to a highly relevant role of BrCs in airway immunity to this complex fungal aeroallergen.

DISCUSSION

BrCs are a unique family of chemosensory cells thus far known to participate in respiratory host defense through their generation of IL-25 and acetylcholine (*6*, *9*, *27*, *29*). Several groups have reported a common transcriptional profile of chemosensory EpCs that includes eicosanoid pathway enzymes (*15*, *25*), but the capacity of any chemosensory EpC to generate eicosanoids and the mechanism(s) that might mediate their generation had not been clarified. Here, we find that two populations of nasal EpCs, residing in the olfactory and respiratory epithelium, share the BrC transcriptional signature including the expression of CysLT biosynthetic enzymes. We demonstrate that BrCs generate CysLTs in response to ATP and to aeroallergens that elicit ATP release (*63*). In each case, CysLT generation was dependent on P2Y2. Together, these findings suggest that CysLT generation is a common chemosensory cell effector mechanism. Last, BrC deficiency results in reduced aeroallergen-induced eosinophilic airway inflammation, implicating BrCs in innate defense mechanisms beyond the recognition of bacterial products.

Our findings provide functional evidence for BrC production of CysLTs. Although previous transcriptional studies have suggested that airway BrCs express the requisite enzymes of the CysLT generation cascade (*2*, *3*, *25*, *27*), the capacity of BrCs to generate CysLTs at levels higher than tissue-resident leukocytes is unexpected. On a per-cell basis, nasal BrCs generated 10-fold more CysLTs than naïve tissue-resident hematopoietic cells. Furthermore, our in vivo data confirm that BrCs are the dominant source of both ATP- and aeroallergen-induced CysLTs released into the nasal airway lumen immediately after inhalation. Although we did not directly compare BrCs with sorted nasal mast cells, we did find that ATP-elicited CysLTs in BrCs and BMMCs are comparable on a per-cell basis, suggesting that BrCs are a potent and relevant source of CysLTs in the airways.

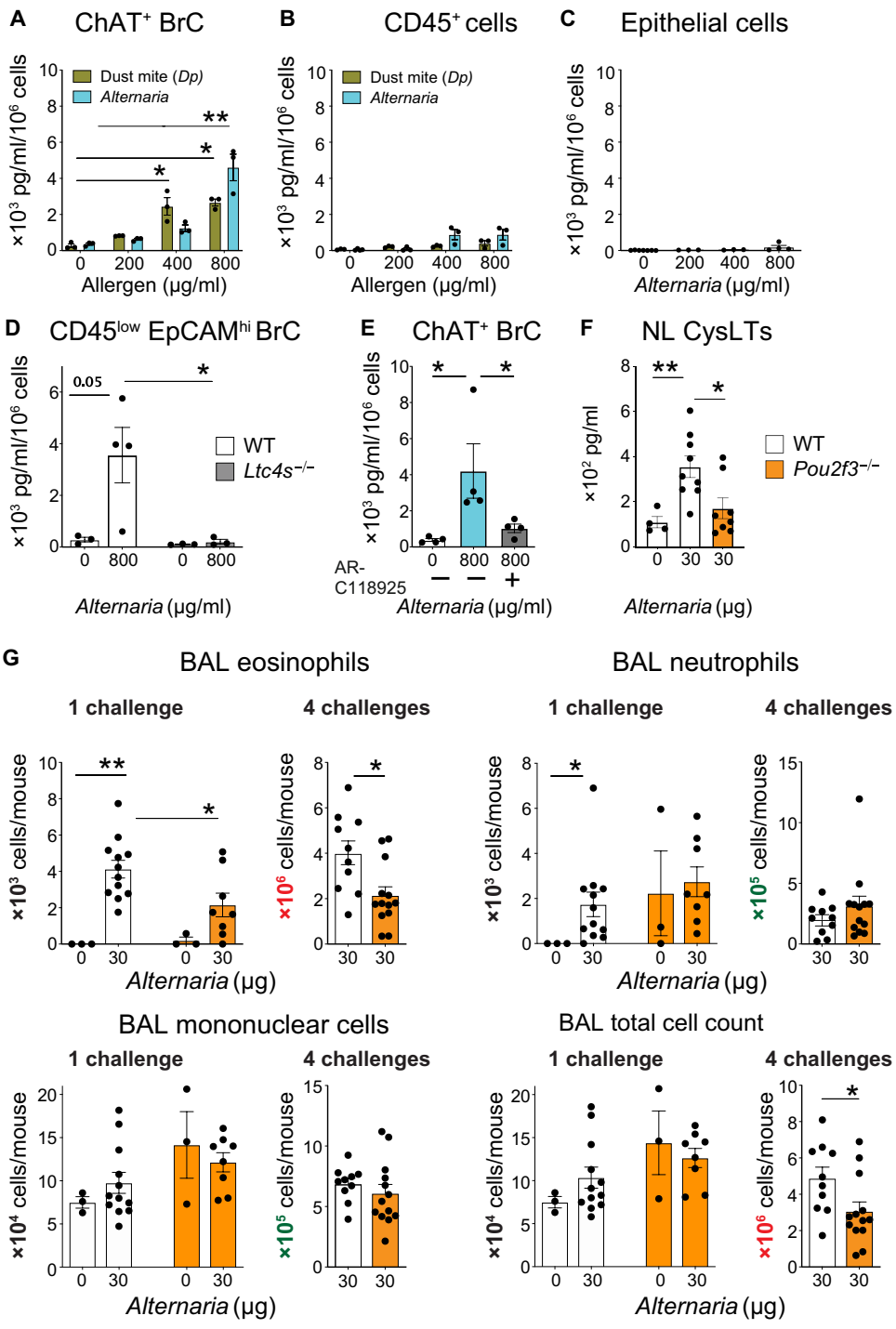

Fig. 4. Allergen-elicited BrC activation triggers airway CysLT generation. (**A** to **C**) ChAT-eGFP$^+$ BrCs, CD45$^+$ cells, and EpCs were isolated from the nasal mucosa of ChAT-eGFP mice and were stimulated ex vivo with the indicated doses of *Alternaria* or *Dp*. (**D**) CD45^{low}EpCAM^{hi} BrCs from WT and *Ltc4s*$^{-/-}$ were stimulated ex vivo with *Alternaria*. (**E**) ChAT-eGFP$^+$ BrCs were pretreated with HBSS with or without the P2Y2 inhibitor AR-C118925 for 15 min and were subsequently stimulated with *Alternaria*. CysLTs were measured in the supernatant at 30 min by ELISA. (**F**) *Alternaria* or HBSS was administered intranasally to naïve WT and *Pou2f3*$^{-/-}$ mice, and nasal lavage was obtained at 30 min. The concentration of CysLTs was measured by ELISA after acetone precipitation. (**G**) WT and *Pou2f3*$^{-/-}$ mice were given one (1 challenge) or four (4 challenges) doses of *Alternaria* intranasally, and the BAL lavage was evaluated 24 or 48 hours after the last challenge. The total number of cells was counted, and differential subsets were evaluated using Diff-Quick. Data are means ± SEM pooled from three independent experiments, each dot is a separate biological replicate, **P* < 0.05, ***P* < 0.01.

Furthermore, both the current study and previous transcriptional analyses of BrCs and tuft cells from the airway and intestine, respectively, have identified the CysLT transcriptional machinery as part of the core profile of chemosensory EpCs (*2*, *3*, *25*, *27*, *34*). Thus, across morphologically and transcriptionally distinct chemosensory subsets, a defining feature is their potential to generate CysLTs, positioning them as key epithelial effectors.

CysLTs are recognized as effector molecules in established airway inflammation for their potent induction of airway vascular permeability and cellular chemotaxis (*68*, *69*). Classically regarded as the products of activated leukocytes, CysLTs are produced in tissue-resident macrophages and mast cells after IgE receptor cross-linking (*40*). CysLTs are also generated by macrophages and mast cells on exposure to microbial stimuli such as IgG-opsonized microbes (*70*, *71*), bacterial peptidoglycan (*72*), dust mites (*42*), zymosan (*73*), and other fungi (*42*). In human airways, CysLTs are generated not only in the setting of IgE cross-linking but also in response to respiratory viruses in exacerbations of asthma (*74*) and in infants without preexisting lung disease (*75*–*78*). Collectively, these studies suggest that CysLT generation is a common response of innate immunity to respiratory pathogens. Our findings demonstrate that extracellular nucleotides in the airway also elicit CysLT generation, further highlighting the conserved nature of this innate pathway in response to diverse respiratory insults.

Although chemosensory EpCs in the airways and intestine share expression of the CysLT biosynthetic pathway, their activating receptors vary between compartments. Canonical taste receptors are more highly expressed in chemosensory tracheal BrCs and thymic chemosensory cells than in intestinal chemosensory tuft cells (*9*, *25*, *27*). Similarly, intestinal chemosensory cells and tracheal BrCs, but not those from the nose, express the succinate receptor 1, a receptor for the tricyclic acid metabolite succinate that is required for the type 2 immune intestinal response to protozoa (*25*, *26*, *53*). This heterogeneity suggests that their sensing apparatus might be modulated to respond to relevant local stimuli.

We found that all airway BrCs express high levels of two purinergic receptors, P2Y2 and P2X4, allowing them to rapidly respond to both luminal signals and EpC damage. Furthermore, we found that inhibition of P2Y2 reduced BrC CysLT generation elicited by ATP, UTP, and *Alternaria*. Previous pharmacologic studies have demonstrated that both MVCs from the olfactory mucosa and SCCs from mouse and human respiratory mucosa are activated by ATP with increases in calcium flux (*17*, *31*, *79*), but an effector function and relevant receptor were not defined. Thus, our findings extend this area significantly by identifying P2Y2 as a previously undescribed BrC sensor for CysLT generation and demonstrating the relevance of this pathway in aeroallergen recognition (fig. S6) (*63*). Because ATP, CysLTs, and the EpC generation of IL-25 are all highly up-regulated in the setting of respiratory viral infections (*75*, *77*, *80*–*83*), P2Y2-dependent BrC activation may play a greater role in airway sensing and immunity than is uncovered here.

Our unbiased transcriptional analysis of nasal cholinergic EpC subsets detected differences in the expression level of key genes between the two nasal BrC subsets including a number of taste receptors, taste receptor signal transduction machinery (*Gnat3*), and the BrC/tuft cell marker DCLK1. However, unsupervised cluster analysis and Euclidean distance measurements demonstrate that olfactory BrCs/MVCs are closer to tracheal BrCs than to noncholinergic EpCs in the nasal mucosa. As previously reported, olfactory BrCs (MVCs) express ChAT (*22*, *28*, *29*), the cation channel TRPM5 (*14*, *20*, *22*, *84*), and the transcription factor Pou2f3 (*18*, *19*, *24*). Furthermore, we find that both nasal olfactory MVCs and nasal respiratory SCCs express core BrC effector programs including *Il25* and CysLT biosynthetic enzymes and are enriched for 73% of the genes reported as a tuft/BrC signature. Thus, we find that the repertoire shared between olfactory BrCs/MVCs and chemosensory EpCs extends beyond the previously reported generation of acetyl choline (*22*, *28*), pointing to shared effector functions and suggesting that these cells should be included in the brush/tuft cell family.

Last, our aeroallergen challenge data confirm a broader importance of BrCs in the airway inflammatory response to aeroallergens. Moreover, because the BrC population expands in the setting of aeroallergen challenge (*27*, *85*) or respiratory viral infection (*86*), our data suggest that BrC-derived CysLTs might also contribute to the enhanced CysLT-generating capacity of the airway in these settings and in diseases such as chronic rhinosinusitis and asthma.

Our study raises several questions that remain unanswered. We previously reported that the innate, *Alternaria*-elicited generation of nasal CysLTs mediates important airway effector functions including: (i) the activation of epithelial goblet cells for mucin release, (ii) the marked dilatation of submucosal vessels, and (iii) the degranulation of mast cells in the nasal submucosa (*44*). Our study demonstrates that MVCs, best characterized for their ability to modulate olfactory responses through calcium depolarization and acetylcholine release (*30*, *31*), can generate CysLTs, but how BrC-derived CysLTs contribute to the function and integrity of the olfactory epithelium remains to be elucidated. In addition, our findings that olfactory BrCs also express high levels of the IL-25 transcript suggest a possible previously unappreciated immune function for these cells. Last, although our in vivo aeroallergen challenge data suggest that BrCs play an important role in aeroallegen-triggered airway inflammation, the specific contribution of BrC effector molecules (IL-25, CysLTs, and prostaglandins) and their potential synergy remains to be elucidated.

Taste receptor signaling in airway BrCs triggers mast cell degranulation and vasodilatation, which depend on BrC activation of trigeminal peptidergic sensory nerves (*28*). However, whether CysLT-dependent nasal mucosal defense depends on sensory neural signaling remains to be determined. CysLTs have been shown to directly activate and modulate the excitability of sensory neurons (*87*, *88*), and several recent studies detected high levels of transcript for the type 2 CysLT receptor in sensory neurons in the vagal (*88*), dorsal root (*89*), and trigeminal ganglia (*90*, *91*). Thus, future studies will be needed to determine whether the protective functions elicited by BrC-derived CysLTs might be transmitted through the nervous system.

MATERIALS AND METHODS

Study design

The aims of this study were to define the capacity of airway BrCs to generate CysLTs and to define activating receptors on BrCs responsible for CysLT generation. We characterized the transcriptional profile of two populations of murine nasal BrCs compared with tracheal BrCs and other EpCs using low-input RNA sequencing on sorted cells from a fluorescent BrC reporter mouse. Using an ex vivo stimulation system, we defined the CysLT-generating capacity of nasal BrCs. Using receptor-specific ligands, inhibitors, and mice with a genetic deletion of the receptor in the ex vivo assay, we defined P2Y2 as an activating GPCR required for CysLT generation. Last, the contribution of BrCs to the total CysLT-generating capacity of the nasal mucosa was evaluated in an in vivo model of ATP and aeroallergen inhalation using a mouse strain lacking nasal BrCs.

Experimental model and mice

ChAT^{BAC}-eGFP [*B6.Cg-Tg*(*RP23–268 L19-EGFP*)*2Mik/J*] mice were purchased from the Jackson Laboratory (Bar Harbor, ME). *Ltc4s*$^{-/-}$ mice were generated on a 129Sv background and backcrossed for 15 generations onto the C57BL/6 background (*92*). *Pou2f3*$^{-/-}$ mice were generated as described previously (*93*) and backcrossed for more than 10 generations onto the C57BL/6 background (*8*, *24*). *P2ry2*$^{-/-}$ mice were described previously (*94*). Age- and sex-matched C57BL/6 mice bred in-house (originally from Charles River Laboratories, Wilmington, MA) were used as controls. Mice were bred and housed in a specific pathogen-free facility at the Brigham and Women's Hospital; pups were weaned between 19 and 28 days after birth. Purchased mice were maintained for at least 4 weeks in the same mouse facility before being used for the experiments. Male and female mice 3 to 8 months of age were used. All mice were housed in groups of four to five mice per cage with a standard 12-hour light/dark cycle and provided food and water ad libitum. All experiments were performed during the day. The use of mice for these studies was in accordance with review and approval by the Animal Care and Use Committee of Brigham and Women's Hospital.

Mouse snout isolation for histology and single-cell preparations

Mouse snouts were harvested from euthanized mice. The lower jaw was dissected with scissors, and the head was separated at the base of the skull. The skin and brain remnant were removed together with the connective tissue surrounding the snout. For histology, the entire snout was fixed in 4% paraformaldehyde for at least 18 hours, changed to phosphate-buffered saline (PBS), and either immediately used for imaging

of the nasal septum or decalcified using 14% (w/v) EDTA in NH_4OH solution (pH 7.2 to 7.4) for 7 to 14 days to prepare histological sections.

Confocal microscopy of nasal septum

For confocal microscopy of the nasal septum, the nasal cavity of $ChAT^{BAC}$-eGFP mice was opened, and the nasal septum was separated. The septum was then permeabilized in a PBS-based blocking buffer containing 0.1% Triton X-100 , 0.1% saponin, 3% bovine serum albumin, and 3% normal donkey serum for 3 hours (*7*). Primary goat anti-GFP (Abcam), primary rabbit anti-DCLK1 antibody (Abcam), and allophycocyanin (APC) anti-mouse CD326 (EpCAM) (BioLegend) antibody were added directly to the blocking buffer for incubation at 4°C for 48 to 72 hours. The specimens were rinsed with PBS containing 0.1% Triton X-100 for 3 to 4 hours, and immunoreactivity to GFP and DCLK1 was detected with secondary donkey anti-goat secondary antibody, Alexa Fluor 488 (Life Technologies), and donkey anti-rabbit secondary antibody, Alexa Fluor 594 (Life Technologies), applied for 72 hours at 4°C. Nuclear staining was performed with Hoechst 33342 nuclear stain (Sigma). The nasal septum was embedded using a glycerol-based coverslipping solution. Images were acquired at the Brigham and Women's Hospital Confocal Microscopy Core Facility using the Zeiss LSM 800 with Airyscan confocal system on a Zeiss Axio Observer Z1 inverted microscope with 10× Zeiss [0.30 numerical aperture (NA)], 20× Zeiss (0.8 NA), and a 63× Zeiss oil (1.4 NA) objectives.

Histology of cross sections

For immunofluorescence of tissue sections, the snouts were sectioned behind the incisors and in between the first three palatal ridges, yielding four coronal sections through the nasal cavity (*44*). The tissue was embedded in paraffin and paraffin-embedded tissue sections (6 μm) were deparaffinized in xylene and rehydrated in ethanol solutions. Heat-induced epitope retrieval was performed in Target Retrieval solution (Dako). Slides were blocked in a PBS-based blocking buffer with 0.1% Triton X-100, 0.1% saponin, 3% bovine serum albumin, and 3% normal donkey serum for 1 hour. Samples were stained with polyclonal rabbit anti-mouse antibodies against Gα-gustducin (Santa Cruz Biotechnology) and a polyclonal goat anti-GFP antibody (Abcam) and a rabbit and goat polyclonal IgG control overnight at 4°C. Immunoreactivity to GFP, DCLK1, and gustducin was detected with secondary donkey anti-goat secondary antibody, Alexa Fluor 488 (Life Technologies), and donkey anti-rabbit secondary antibody, Alexa Fluor 594 (Life Technologies), applied for 2 hours at room temperature. Nuclear staining was performed with Hoechst 33342 nuclear stain (Sigma).

Single-cell preparations for ex vivo cell stimulation and RNA sequencing

For single-cell preparations, the ethmoid bone overlying the nasal cavity was removed to expose the nasal mucosa, and the whole snout was incubated in prewarmed PBS solution containing dispase (16 U/ml; Gibco) and deoxyribonuclease I (DNase I; 20 μg/ml; Sigma) for 30 to 40 min at room temperature with gentle shaking. The dispase activity was quenched by dilution with cold Dulbecco's modified Eagle's medium (DMEM) and 5% fetal bovine serum (FBS). The mucosa of the whole nasal cavity was carefully scraped off with scalpel under a dissecting microscope. The epithelium, together with the remainders of the nasal septum, was incubated in Hepes-Tyrode's buffer without calcium (Boston BioProducts, Boston, MA) containing papain (20 μl/ml, 28 U/mg; Sigma), L-cysteine (10 μl/ml, 25 mg/ml; Sigma), and DNase I (20 μg/ml; Sigma) for 30 min at 37°C with gentle agitation. Papain digestion was terminated with Tyrode's solution (Boston BioProducts) with leupeptin (2 μl/ml, 5 mg/ml; Sigma). The digested tissue was vortexed for 30 s and thoroughly triturated using a 21-gauge needle. The digested cells were passed through a 100-μm filter, washed once, and stained using monoclonal antibodies against CD45 and EpCAM, followed by dead cell exclusion with propidium iodide before sorting. BrCs were identified as $CD45^{low/-}EpCAM^{+}eGFP^{+}$ cells. Nasal EpCs were identified as $CD45^{low/-}EpCAM^{+}eGFP^{-}$ cells, and $CD45^{+}$ cells were separately sorted. For RNA sequencing experiments, the BrCs were subdivided into two populations: Olfactory BrCs were defined as $CD45^{low/-}EpCAM^{+}eGFP^{-}FSC^{low}SSC^{low}$ BrCs, whereas respiratory BrC were defined as $CD45^{low/-}EpCAM^{+}eGFP^{-}FSC^{hi}SSC^{hi}$ (Fig. 1A). Sorted $CD45^{+}$ cells were further characterized on the basis of their expression of CD11b, CD11c, CD4, CD8, major histocompatibility complex II, kit, and Fcεr1 (fig. S3). In a separate set of experiments, BrCs were isolated from WT C57BL/6, $Ltc4s^{-/-}$, $Pou2f3^{-/-}$, and $P2ry2^{-/-}$ mice based on their high expression of EpCAM and low expression of CD45 (fig. S5). Cells were sorted at the Brigham and Women's Human Immunology Flow Core using a BD FACSAria Fusion cell sorter. For RNA sequencing, at least 300 but no more than 500 cells from one naïve digested mouse nose were sorted into TCL buffer (Qiagen) supplemented with RNAprotect Cell Reagent (Qiagen). Tracheal BrCs and tracheal EpCs were sorted as previously described (*27*).

Ex vivo stimulation of nasal BrCs

Sorted EpCs and BrCs were plated in DMEM-based EpC proliferation media, which includes DMEM/F-12, 5% FBS, 10 mM Hepes, penicillin (100 U/ml), streptomycin (100 μg/ml), insulin (10 μg/ml), transferrin (5 μg/ml), epithermal growth factor (25 ng/ml), cholera toxin (0.1 μg/ml), bovine pituitary extract (30 μg/ml), bovine serum albumin (10 μg/ml), 100 nM retinoic acid, and amphotericin B (0.25 μg/ml) (*95*). Sorted $CD45^{+}$ cells were reconstituted in R10 media [RPMI 1640 medium containing 10% (v/v) FBS, 2 mM L-glutamine, 0.1 mM nonessential amino acids, penicillin (100 U/ml), streptomycin (100 μg/ml), and 1% culture supernatant from Chinese hamster ovary cells expressing mouse IL-3 (*44*)]. The cells were plated into 96-well culture plates at a concentration of 400,000 cells/ml in 50 μl of media per well and rested for 18 hours. The cells were stimulated with *Alternaria* (200 to 800 μg/ml; lot no. 151774), *Dp* (200 to 800 μg/ml; lot no. 45415) (both from Greer Laboratories, Lenoir, NC), A23187 (0.1 to 10 mM; Cayman), ATPγS (0.1 to 10 mM; Abcam), or UTP (0.5 to 2 mM; Sigma) in 50 μl of Hanks' balanced salt solution (HBSS) with calcium and magnesium for 30 min. For inhibition experiments, the cells were pretreated with HBSS with calcium and magnesium with or without the FLAP inhibitor MK-886 (1 μM; Cayman), P2Y2 receptor inhibitor AR-C 118925XX (10 μM; Tocris Bioscience), or P2X4 receptor inhibitor 5-BDBD (10 μM; Tocris Bioscience) for 15 min before the stimulus was added. After stimulation, the reaction was stopped by centrifugation at 350*g* for 5 min at 4°C, and the supernatants were retained for assays of CysLTs.

LDH release assay

Isolated BrCs were incubated in 96-well plates in 100 μl of DMEM-based EpC proliferation media at a concentration of 14,000 to 15,000 cells per well for 1 or 18 hours. Both DMEM without additives and DMEM-based EpC proliferation media containing serum were used as controls to account for background due to FBS-related

LDH activity (*96*). LDH release was measured using the LDH Cytotoxicity Assay Kit (Thermo Fisher Scientific) by adding either 10 μl of lysis buffer or 10 μl of sterile, ultrapure water to wells containing BrCs. The plate was further incubated at 37°C and 5% CO_2 for 45 min. Each sample (50 μl), serum-free medium, and proliferation medium were transferred to a new plate and mixed with 50 μl of reaction mixture. After 30 min of incubation at room temperature protected from light, the reaction was stopped by adding 50 μl of stop solution. The absorbance was measured at 490 and 680 nm, with 490 nm representing LDH-induced red formazan conversion and 680 nm standing for machine background. The results of the LDH assay are presented as optical density differences between 490 and 680 nm measurements.

In vivo CysLT generation assay

Mice received a single intranasal application of *Alternaria* culture filtrate or ATPγS after anesthesia with an intraperitoneal injection of ketamine (10 mg/kg) and xylazine (20 mg/kg) for full sedation. The aeroallergen extract and ATPγS were delivered in a total volume of 20 μl of sterile PBS. Mice were euthanized 30 min after the intranasal challenge with isoflurane overdose, and nasal lavage was performed with 200 μl of PBS through a tracheal opening. The nasal lavage fluid protein was precipitated with ice-cold acetone, and after high-speed centrifugation, the lipid fraction was retrieved for CysLT measurements. Mice of a given genotype were randomized to treatment dose, and challenges were performed in groups organized by genotype and treatment dose.

Aeroallergen challenge for BAL fluid analysis

Mice received 30 μg of *Alternaria* or PBS intranasally once for an analysis of BAL fluid 24 hours later or four times over 9 days for BAL fluid analysis 48 hours after the last challenge. After euthanasia, the trachea was cannulated, and BAL was obtained by three repeated lavages with 0.75 ml of PBS with 1 mM EDTA. The BAL fluid was centrifuged at 500*g* for 5 min. Cells were resuspended in 0.2 ml of PBS, and the total cells were counted manually with a hemocytometer. For the differential cell counts of macrophages, neutrophils, and eosinophils, the cells were cytospun onto a glass slide and stained with Diff-Quik. Cell types in a total of 200 cells were identified by morphologic criteria (*97*).

BMMC culture and stimulation

BMMCs were generated as previously described (*92*). Briefly, bone marrow was collected from femurs and tibiae of mice and cultured for 4 to 6 weeks in R10 media described previously. The culture medium for the BMMC was changed every week, and the cell density was adjusted to 3×10^5/ml at every passage. After 4 weeks, more than 97% of the cells were BMMCs as assessed by staining with Wright-Giemsa and toluidine blue.

BMMCs were harvested from culture and plated at a concentration of 400,000 cells/ml in 50 μl of R10 media per well and rested for 2 hours. The cells were stimulated with ATPγS (0.1 to 10 mM; Abcam) in 50 μl of HBSS with calcium and magnesium for 30 min, centrifuged at 350*g* for 5 min at 4°C, and the supernatants were retained for enzyme-linked immunosorbent assay (ELISA) assays to measure CysLT generation.

CysLT detection

CysLT generation in the supernatants of BrCs, EpCs, $CD45^+$ sorted cells, cultured BMMCs, and acetone-precipitated nasal lavage fluid was measured by a commercially available enzyme immunoassay (ELISA) according to the manufacturer's protocol (Cayman) based on competition between CysLTs and CysLT-acetylcholinesterase conjugate for a limited amount of CysLT ELISA Monoclonal Antibody. The lower limit of detection was 60 pg/ml, and the following reported reactivity are leukotriene C_4 (100%), leukotriene D_4 (100%), leukotriene E_4 (79%), 5,6-DiHETE (3.7%), leukotriene B_4 (1.3%), 5(S)-HETE (0.04%), and arachidonic acid (<0.01%).

Low-input RNA sequencing

Cells from nasal single-cell suspensions were processed at the Broad Institute Technology Labs using low-input eukaryotic Smart-seq2. Briefly, Smart-seq2 libraries were sequenced on an Illumina NextSeq 500 using a High-Output kit to generate 2 × 25-bp reads (plus dual index reads). Each sample's sequences were aligned using STAR v2.4.2a (*98*) and parameters are as follows: --twopassMode Basic, -- alignIntronMax 1000000, --alignMatesGapMax 1000000, --sjdbScore 2, --quantMode TranscriptomeSAM, --sjdbOverhang 24. Alignments were processed using Picard v1.1073 tools to add read groups and other sequencing information, reorder the BAM file to the reference, and mark duplicate sequences. The data were assessed for quality using RNA-SeQC (*99*). RNA sequencing results were analyzed using R Bioconductor. Raw counts were generated using the featureCounts function of Rsubread (*100*). Raw input was used for normalization and differential expression analysis by DeSeq2 software. STAR-aggregated mappings on a per-gene basis were used as raw input for normalization by DESeq2 software (*101*). Any genes with a mean normalized read count of <10 in any BrC subset were removed from analysis. Genes were considered to be significantly differentially regulated based on a fold change in expression of >2-fold and a false discovery rate of <0.05 based on a Benjamini-Hochberg adjusted *P* value to correct for multiple comparisons. Principal components analysis was conducted using the top 100 differentially regulated genes by false discovery rate.

Statistics

Analysis was performed with GraphPad Prism software (version 8, GraphPad, La Jolla, CA). Nonparametric two-sided Mann-Whitney and unpaired *t* tests were used to determine significance in pairwise comparison of responses in the in vivo and ex vivo stimulation models. For dose responses, the overall significance was determined using a one-way analysis of variance (ANOVA) or Kruskal-Wallis tests, and pairwise multiple comparisons was performed with Dunn's tests. A value of $P < 0.05$ was considered significant. Sample sizes were not predetermined by statistical methods.

SUPPLEMENTARY MATERIALS

immunology.sciencemag.org/cgi/content/full/5/43/eaax7224/DC1

Fig. S1. Nasal ChAT-eGFP$^+$ cells share the tuft cell signature.

Fig. S2. Nasal BrCs are enriched for phosphatidylinositol-phospholipase signaling and CysLT biosynthetic pathway transcripts.

Fig. S3. BrCs are the dominant source of CysLTs in the naïve nasal mucosa.

Fig. S4. Taste receptors are highly expressed in tracheal and respiratory nasal but not olfactory nasal BrCs.

Fig. S5. CD45 is expressed on nasal BrCs.

Fig. S6. Aeroallergen-triggered pathways of BrC activation.

Table S1. Reagents.

Table S2. Raw data in Excel file.

View/request a protocol for this paper from *Bio-protocol*.

REFERENCES AND NOTES

1. B. N. Lambrecht, H. Hammad, Allergens and the airway epithelium response: Gateway to allergic sensitization. *J. Allergy Clin. Immunol.* **134**, 499–507 (2014).
2. D. T. Montoro, A. L. Haber, M. Biton, V. Vinarsky, B. Lin, S. E. Birket, F. Yuan, S. Chen, H. M. Leung, J. Villoria, N. Rogel, G. Burgin, A. M. Tsankov, A. Waghray, M. Slyper, J. Waldman, L. Nguyen, D. Dionne, O. Rozenblatt-Rosen, P. R. Tata, H. Mou, M. Shivaraju, H. Bihler, M. Mense, G. J. Tearney, S. M. Rowe, J. F. Engelhardt, A. Regev, J. Rajagopal, A revised airway epithelial hierarchy includes CFTR-expressing ionocytes. *Nature* **560**, 319–324 (2018).
3. L. W. Plasschaert, R. Žilionis, R. Choo-Wing, V. Savova, J. Knehr, G. Roma, A. M. Klein, A. B. Jaffe, A single-cell atlas of the airway epithelium reveals the CFTR-rich pulmonary ionocyte. *Nature* **560**, 377–381 (2018).
4. J. Ordovas-Montanes, D. F. Dwyer, S. K. Nyquist, K. M. Buchheit, M. Vukovic, C. Deb, M. H. Wadsworth II, T. K. Hughes, S. W. Kazer, E. Yoshimoto, K. N. Cahill, N. Bhattacharyya, H. R. Katz, B. Berger, T. M. Laidlaw, J. A. Boyce, N. A. Barrett, A. K. Shalek, Allergic inflammatory memory in human respiratory epithelial progenitor cells. *Nature* **560**, 649–654 (2018).
5. G. Krasteva, W. Kummer, "Tasting" the airway lining fluid. *Histochem. Cell Biol.* **138**, 365–383 (2012).
6. J. von Moltke, M. Ji, H.-E. Liang, R. M. Locksley, Tuft-cell-derived IL-25 regulates an intestinal ILC2-epithelial response circuit. *Nature* **529**, 221–225 (2016).
7. M. R. Howitt, S. Lavoie, M. Michaud, A. M. Blum, S. V. Tran, J. V. Weinstock, C. A. Gallini, K. Redding, R. F. Margolskee, L. C. Osborne, D. Artis, W. S. Garrett, Tuft cells, taste-chemosensory cells, orchestrate parasite type 2 immunity in the gut. *Science* **351**, 1329–1333 (2016).
8. F. Gerbe, E. Sidot, D. J. Smyth, M. Ohmoto, I. Matsumoto, V. Dardalhon, P. Cesses, L. Garnier, M. Pouzolles, B. Brulin, M. Bruschi, Y. Harcus, V. S. Zimmermann, N. Taylor, R. M. Maizels, P. Jay, Intestinal epithelial tuft cells initiate type 2 mucosal immunity to helminth parasites. *Nature* **529**, 226–230 (2016).
9. G. Krasteva, B. Böttger, A. Hansen, K. T. Anderson, H. Alimohammadi, W. L. Silver, Cholinergic chemosensory cells in the trachea regulate breathing. *Proc. Natl. Acad. Sci. U.S.A.* **108**, 9478–9483 (2011).
10. T. E. Finger, B. Böttger, A. Hansen, K. T. Anderson, H. Alimohammadi, W. L. Silver, Solitary chemoreceptor cells in the nasal cavity serve as sentinels of respiration. *Proc. Natl. Acad. Sci. U.S.A.* **100**, 8981–8986 (2003).
11. M. F. DiMaio, M. Kattan, D. Ciurea, J. Gil, R. Dische, Brush cells in the human fetal trachea. *Pediatr. Pulmonol.* **8**, 40–44 (1990).
12. L. Reid, B. Meyrick, V. B. Antony, L. Y. Chang, J. D. Crapo, H. Y. Reynolds, The mysterious pulmonary brush cell: A cell in search of a function. *Am. J. Respir. Crit. Care Med.* **172**, 136–139 (2005).
13. M. Ohmoto, I. Matsumoto, A. Yasuoka, Y. Yoshihara, K. Abe, Genetic tracing of the gustatory and trigeminal neural pathways originating from T1R3-expressing taste receptor cells and solitary chemoreceptor cells. *Mol. Cell. Neurosci.* **38**, 505–517 (2008).
14. W. Lin, T. Ogura, R. F. Margolskee, T. E. Finger, D. Restrepo, TRPM5-expressing solitary chemosensory cells respond to odorous irritants. *J. Neurophysiol.* **99**, 1451–1460 (2008).
15. C. Bezencon, A. Fürholz, F. Raymond, R. Mansourian, S. Métairon, J. Le Coutre, S. Damak, Murine intestinal cells expressing Trpm5 are mostly brush cells and express markers of neuronal and inflammatory cells. *J. Comp. Neurol.* **509**, 514–525 (2008).
16. S. Kaske, G. Krasteva, P. König, W. Kummer, T. Hofmann, T. Gudermann, V. Chubanov, TRPM5, a taste-signaling transient receptor potential ion-channel, is a ubiquitous signaling component in chemosensory cells. *BMC Neurosci.* **8**, 49 (2007).
17. B. D. Gulbransen, T. R. Clapp, T. E. Finger, S. C. Kinnamon, Nasal solitary chemoreceptor cell responses to bitter and trigeminal stimulants in vitro. *J. Neurophysiol.* **99**, 2929–2937 (2008).
18. M. Ohmoto, T. Yamaguchi, J. Yamashita, A. A. Bachmanov, J. Hirota, I. Matsumoto, Pou2f3/Skn-1a is necessary for the generation or differentiation of solitary chemosensory cells in the anterior nasal cavity. *Biosci. Biotechnol. Biochem.* **77**, 2154–2156 (2013).
19. J. Yamashita, M. Ohmoto, T. Yamaguchi, I. Matsumoto, J. Hirota, Skn-1a/Pou2f3 functions as a master regulator to generate Trpm5-expressing chemosensory cells in mice. *PLOS ONE* **12**, e0189340 (2017).
20. A. Hansen, T. E. Finger, Is TrpM5 a reliable marker for chemosensory cells? Multiple types of microvillous cells in the main olfactory epithelium of mice. *BMC Neurosci.* **9**, 115 (2008).
21. W. Lin, E. A. Ezekwe Jr., Z. Zhao, E. R. Liman, D. Restrepo, TRPM5-expressing microvillous cells in the main olfactory epithelium. *BMC Neurosci.* **9**, 114 (2008).
22. T. Ogura, S. A. Szebenyi, K. Krosnowski, A. Sathyanesan, J. Jackson, W. Lin, Cholinergic microvillous cells in the mouse main olfactory epithelium and effect of acetylcholine on olfactory sensory neurons and supporting cells. *J. Neurophysiol.* **106**, 1274–1287 (2011).
23. F. Genovese, M. Tizzano, Microvillous cells in the olfactory epithelium express elements of the solitary chemosensory cell transduction signaling cascade. *PLOS ONE* **13**, e0202754 (2018).
24. T. Yamaguchi, J. Yamashita, M. Ohmoto, I. Aoudé, T. Ogura, W. Luo, A. A. Bachmanov, W. Lin, I. Matsumoto, J. Hirota, Skn-1a/Pou2f3 is required for the generation of Trpm5-expressing microvillous cells in the mouse main olfactory epithelium. *BMC Neurosci.* **15**, 13 (2014).
25. M. S. Nadjsombati, J. W. McGinty, M. R. Lyons-Cohen, J. B. Jaffe, L. DiPeso, C. Schneider, C. N. Miller, J. L. Pollack, G. A. N. Gowda, M. F. Fontana, D. J. Erle, M. S. Anderson, R. M. Locksley, D. Raftery, J. von Moltke, Detection of Succinate by Intestinal Tuft Cells Triggers a Type 2 Innate Immune Circuit. *Immunity* **49**, 33–41.e7 (2018).
26. C. Schneider, C. E. O'Leary, J. Moltke, H.-E. Liang, Q. Y. Ang, P. J. Turnbaugh, S. Radhakrishnan, M. Pellizzon, A. Ma, R. M. Locksley, A Metabolite-Triggered Tuft Cell-ILC2 Circuit Drives Small Intestinal Remodeling. *Cell* **174**, 271–284.e14 (2018).
27. L. G. Bankova, D. F. Dwyer, E. Yoshimoto, S. Ualiyeva, J. W. Mc Ginty, H. Raff, J. von Moltke, Y. Kanaoka, K. F. Austen, N. A. Barrett, The cysteinyl leukotriene 3 receptor regulates expansion of IL-25-producing airway brush cells leading to type 2 inflammation. *Sci. Immunol.* **3**, eaat9453 (2018).
28. C. J. Saunders, M. Christensen, T. E. Finger, M. Tizzano, Cholinergic neurotransmission links solitary chemosensory cells to nasal inflammation. *Proc. Natl. Acad. Sci. U.S.A.* **111**, 6075–6080 (2014).
29. G. Krasteva, B. J. Canning, T. Papadakis, W. Kummer, Cholinergic brush cells in the trachea mediate respiratory responses to quorum sensing molecules. *Life Sci.* **91**, 992–996 (2012).
30. K. Lemons, Z. Fu, I. Aoudé, T. Ogura, J. Sun, J. Chang, K. Mbonu, I. Matsumoto, H. Arakawa, W. Lin, Lack of TRPM5-expressing microvillous cells in mouse main olfactory epithelium leads to impaired odor-evoked responses and olfactory-guided behavior in a challenging chemical environment. *eNeuro* **4**, ENEURO.0135-17.2017 (2017).
31. Z. Fu, T. Ogura, W. Luo, W. Lin, ATP and odor mixture activate TRPM5-expressing microvillous cells and potentially induce acetylcholine release to enhance supporting cell endocytosis in mouse main olfactory epithelium. *Front. Cell. Neurosci.* **12**, 71 (2018).
32. D. Prawitt, M. K. Monteilh-Zoller, L. Brixel, C. Spangenberg, B. Zabel, A. Fleig, R. Penner, TRPM5 is a transient Ca^{2+}–activated cation channel responding to rapid changes in $[Ca^{2+}]i$. *Proc. Natl. Acad. Sci. U.S.A.* **100**, 15166–15171 (2003).
33. W. M. Yau, J. A. Dorsett, M. L. Youther, Calcium-dependent stimulation of acetylcholine release by substance P and vasoactive intestinal polypeptide. *Eur. J. Pharmacol.* **120**, 241–243 (1986).
34. A. L. Haber, M. Biton, N. Rogel, R. H. Herbst, K. Shekhar, C. Smillie, G. Burgin, T. M. Delorey, M. R. Howitt, Y. Katz, I. Tirosh, S. Beyaz, D. Dionne, M. Zhang, R. Raychowdhury, W. S. Garrett, O. Rozenblatt-Rosen, H. N. Shi, O. Yilmaz, R. J. Xavier, A. Regev, A single-cell survey of the small intestinal epithelium. *Nature* **551**, 333–339 (2017).
35. T. Yoshimoto, R. J. Soberman, B. Spur, K. F. Austen, Properties of highly purified leukotriene C4 synthase of guinea pig lung. *J. Clin. Invest.* **81**, 866–871 (1988).
36. B. K. Lam, W. F. Owen Jr., K. F. Austen, R. J. Soberman, The identification of a distinct export step following the biosynthesis of leukotriene C4 by human eosinophils. *J. Biol. Chem.* **264**, 12885–12889 (1989).
37. C. A. Rouzer, B. Samuelsson, Reversible, calcium-dependent membrane association of human leukocyte 5-lipoxygenase. *Proc. Natl. Acad. Sci. U.S.A.* **84**, 7393–7397 (1987).
38. E. A. Nalefski, L. A. Sultzman, D. M. Martin, R. W. Kriz, P. S. Towler, J. L. Knopf, J. D. Clark, Delineation of two functionally distinct domains of cytosolic phospholipase A2, a regulatory Ca^{2+}-dependent lipid-binding domain and a Ca^{2+}-independent catalytic domain. *J. Biol. Chem.* **269**, 18239–18249 (1994).
39. O. H. Choi, J. H. Lee, T. Kassessinoff, J. R. Cunha-Melo, S. V. Jones, M. A. Beaven, Antigen and carbachol mobilize calcium by similar mechanisms in a transfected mast cell line (RBL-2H3 cells) that expresses ml muscarinic receptors. *J. Immunol.* **151**, 5586–5595 (1993).
40. E. Razin, J. M. Mencia-Huerta, R. L. Stevens, R. A. Lewis, F. T. Liu, E. Corey, K. F. Austen, IgE-mediated release of leukotriene C4, chondroitin sulfate E proteoglycan, beta-hexosaminidase, and histamine from cultured bone marrow-derived mouse mast cells. *J. Exp. Med.* **157**, 189–201 (1983).
41. S. Suram, T. A. Gangelhoff, P. R. Taylor, M. Rosas, G. D. Brown, J. V. Bonventre, S. Akira, S. Uematsu, D. L. Williams, R. C. Murphy, C. C. Leslie, Pathways regulating cytosolic phospholipase A2 activation and eicosanoid production in macrophages by Candida albicans. *J. Biol. Chem.* **285**, 30676–30685 (2010).
42. N. A. Barrett, A. Maekawa, O. M. Rahman, K. F. Austen, Y. Kanaoka, Dectin-2 recognition of house dust mite triggers cysteinyl leukotriene generation by dendritic cells. *J. Immunol.* **182**, 1119–1128 (2009).
43. M. W. Buczynski, D. L. Stephens, R. C. Bowers-Gentry, A. Grkovich, R. A. Deems, E. A. Dennis, TLR-4 and sustained calcium agonists synergistically produce eicosanoids independent of protein synthesis in RAW264.7 cells. *J. Biol. Chem.* **282**, 22834–22847 (2007).
44. L. G. Bankova, J. Lai, E. Yoshimoto, J. A. Boyce, K. F. Austen, Y. Kanaoka, N. A. Barrett, Leukotriene E4 elicits respiratory epithelial cell mucin release through the G-protein-coupled receptor, GPR99. *Proc. Natl. Acad. Sci. U.S.A.* **113**, 6242–6247 (2016).
45. Y. N. Tallini, B. Shui, K. S. Greene, K. Y. Deng, R. Doran, P. J. Fisher, W. Zipfel, M. I. Kotlikoff, BAC transgenic mice express enhanced green fluorescent protein in central and peripheral cholinergic neurons. *Physiol. Genomics* **27**, 391–397 (2006).

46. T. Ogura, K. Krosnowski, L. Zhang, M. Bekkerman, W. Lin, Chemoreception regulates chemical access to mouse vomeronasal organ: Role of solitary chemosensory cells. *PLOS ONE* **5**, e11924 (2010).
47. Y. Zhang, M. A. Hoon, J. Chandrashekar, K. L. Mueller, B. Cook, D. Wu, C. S. Zuker, N. J. P. Ryba, Coding of sweet, bitter, and umami tastes: Different receptor cells sharing similar signaling pathways. *Cell* **112**, 293–301 (2003).
48. P. Topilko, S. Schneider-Maunoury, G. Levi, A. Baron-Van Evercooren, A. B. Chennoufi, T. Seitanidou, C. Babinet, P. Charnay, Krox-20 controls myelination in the peripheral nervous system. *Nature* **371**, 796–799 (1994).
49. N. Du, H. Kwon, P. Li, E. E. West, J. Oh, W. Liao, Z. Yu, M. Ren, W. J. Leonard, EGR2 is critical for peripheral naive T-cell differentiation and the T-cell response to influenza. *Proc. Natl. Acad. Sci. U.S.A.* **111**, 16484–16489 (2014).
50. V. Lazarevic, A. J. Zullo, M. N. Schweitzer, T. L. Staton, E. M. Gallo, G. R. Crabtree, L. H. Glimcher, The gene encoding early growth response 2, a target of the transcription factor NFAT, is required for the development and maturation of natural killer T cells. *Nat. Immunol.* **10**, 306–313 (2009).
51. J. H. Lee, T. Tammela, M. Hofree, J. Choi, N. D. Marjanovic, S. Han, D. Canner, K. Wu, M. Paschini, D. H. Bhang, T. Jacks, A. Regev, C. F. Kim, Anatomically and Functionally Distinct Lung Mesenchymal Populations Marked by Lgr5 and Lgr6. *Cell* **170**, 1149–1163.e12 (2017).
52. C. E. O'Leary, C. Schneider, R. M. Locksley, Tuft Cells-Systemically Dispersed Sensory Epithelia Integrating Immune and Neural Circuitry. *Annu. Rev. Immunol.* **37**, 47–72 (2018).
53. W. Lei, W. Ren, M. Ohmoto, J. F. Urban Jr., I. Matsumoto, R. F. Margolskee, P. Jiang, Activation of intestinal tuft cell-expressed Sucnr1 triggers type 2 immunity in the mouse small intestine. *Proc. Natl. Acad. Sci. U.S.A.* **115**, 5552–5557 (2018).
54. M. Rafehi, J. C. Burbiel, I. Y. Attah, A. Abdelrahman, C. E. Müller, Synthesis, characterization, and in vitro evaluation of the selective P2Y2 receptor antagonist AR-C118925. *Purinergic Signal* **13**, 89–103 (2017).
55. D. Communi, R. Janssens, N. Suarez-Huerta, B. Robaye, J.-M. Boeynaems, Advances in signalling by extracellular nucleotides. the role and transduction mechanisms of P2Y receptors. *Cell. Signal.* **12**, 351–360 (2000).
56. W. G. Junger, Immune cell regulation by autocrine purinergic signalling. *Nat. Rev. Immunol.* **11**, 201–212 (2011).
57. K. A. Jacobson, R. Balasubramanian, F. Deflorian, Z. G. Gao, G protein-coupled adenosine (P1) and P2Y receptors: Ligand design and receptor interactions. *Purinergic Signal* **8**, 419–436 (2012).
58. K. D. Lustig, A. K. Shiau, A. J. Brake, D. Julius, Expression cloning of an ATP receptor from mouse neuroblastoma cells. *Proc. Natl. Acad. Sci. U.S.A.* **90**, 5113–5117 (1993).
59. C. Coddou, Z. Yan, T. Obsil, J. P. Huidobro-Toro, S. S. Stojilkovic, Activation and regulation of purinergic P2X receptor channels. *Pharmacol. Rev.* **63**, 641–683 (2011).
60. C. Feng, A. G. Mery, E. M. Beller, C. Favot, J. A. Boyce, Adenine nucleotides inhibit cytokine generation by human mast cells through a Gs-coupled receptor. *J. Immunol.* **173**, 7539–7547 (2004).
61. E. A. Mellor, K. F. Austen, J. A. Boyce, Cysteinyl leukotrienes and uridine diphosphate induce cytokine generation by human mast cells through an interleukin 4-regulated pathway that is inhibited by leukotriene receptor antagonists. *J. Exp. Med.* **195**, 583–592 (2002).
62. C. Ledderose, K. Liu, Y. Kondo, C. J. Slubowski, T. Dertnig, S. Denicoló, M. Arbab, J. Hubner, K. Konrad, M. Fakhari, J. A. Lederer, S. C. Robson, G. A. Visner, W. G. Junger, Purinergic P2X4 receptors and mitochondrial ATP production regulate T cell migration. *J. Clin. Invest.* **128**, 3583–3594 (2018).
63. S. M. O'Grady, N. Patil, T. Melkamu, P. J. Maniak, C. Lancto, H. Kita, ATP release and Ca^{2+} signalling by human bronchial epithelial cells following Alternaria aeroallergen exposure. *J. Physiol.* **591**, 4595–4609 (2013).
64. S. Ramu, M. Menzel, L. Bjermer, C. Andersson, H. Akbarshahi, L. Uller, Allergens produce serine proteases-dependent distinct release of metabolite DAMPs in human bronchial epithelial cells. *Clin. Exp. Allergy* **48**, 156–166 (2018).
65. K. R. Bartemes, K. Iijima, T. Kobayashi, G. M. Kephart, A. N. McKenzie, H. Kita, IL-33-responsive lineage- CD25+ CD44(hi) lymphoid cells mediate innate type 2 immunity and allergic inflammation in the lungs. *J. Immunol.* **188**, 1503–1513 (2012).
66. T. A. Doherty, N. Khorram, J. E. Chang, H. K. Kim, P. Rosenthal, M. Croft, D. H. Broide, STAT6 regulates natural helper cell proliferation during lung inflammation initiated by Alternaria. *Am. J. Phys. Lung Cell. Mol. Phys.* **303**, L577–L588 (2012).
67. T. A. Doherty, N. Khorram, K. Sugimoto, D. Sheppard, P. Rosenthal, J. Y. Cho, A. Pham, M. Miller, M. Croft, D. H. Broide, Alternaria induces STAT6-dependent acute airway eosinophilia and epithelial FIZZ1 expression that promotes airway fibrosis and epithelial thickness. *J. Immunol.* **188**, 2622–2629 (2012).
68. L. G. Bankova, J. A. Boyce, A new spin on mast cells and cysteinyl leukotrienes: Leukotriene E_4 activates mast cells in vivo. *J. Allergy Clin. Immunol.* **142**, 1056–1057 (2018).
69. M. Peters-Golden, W. R. Henderson Jr., Leukotrienes. *N. Engl. J. Med.* **357**, 1841–1854 (2007).
70. H.-E. Claesson, J. Å. Lindgren, B. Gustafsson, Opsonized bacteria stimulate leukotriene synthesis in human leukocytes. *Biochim. Biophys. Acta* **836**, 361–367 (1985).
71. C. A. Rouzer, W. A. Scott, Z. A. Cohn, P. Blackburn, J. M. Manning, Mouse peritoneal macrophages release leukotriene C in response to a phagocytic stimulus. *Proc. Natl. Acad. Sci. U.S.A.* **77**, 4928–4932 (1980).
72. J. D. McCurdy, T. J. Olynych, L. H. Maher, J. S. Marshall, Cutting edge: Distinct Toll-like receptor 2 activators selectively induce different classes of mediator production from human mast cells. *J. Immunol.* **170**, 1625–1629 (2003).
73. T. J. Olynych, D. L. Jakeman, J. S. Marshall, Fungal zymosan induces leukotriene production by human mast cells through a dectin-1-dependent mechanism. *J. Allergy Clin. Immunol.* **118**, 837–843 (2006).
74. J. M. Drazen, J. O'Brien, D. Sparrow, S. T. Weiss, M. A. Martins, E. Israel, C. H. Fanta, Recovery of leukotriene E4 from the urine of patients with airway obstruction. *Am. Rev. Respir. Dis.* **146**, 104–108 (1992).
75. L. Da Dalt, S. Callegaro, S. Carraro, B. Andreola, M. Corradi, E. Baraldi, Nasal lavage leukotrienes in infants with RSV bronchiolitis. *Pediatr. Allergy Immunol.* **18**, 100–104 (2007).
76. Y. Sznajer, J. Y. Westcott, S. E. Wenzel, B. Mazer, M. Tucci, B. J. Toledano, Airway eicosanoids in acute severe respiratory syncytial virus bronchiolitis. *J. Pediatr.* **145**, 115–118 (2004).
77. G. Piedimonte, G. Renzetti, A. Auais, A. D. Marco, S. Tripodi, F. Colistro, A. Villani, V. D. Ciommo, R. Cutrera, Leukotriene synthesis during respiratory syncytial virus bronchiolitis: Influence of age and atopy. *Pediatr. Pulmonol.* **40**, 285–291 (2005).
78. S. M. van Schaik, D. A. Tristram, I. S. Nagpal, K. M. Hintz, R. C. Welliver II, R. C. Welliver, Increased production of IFN-gamma and cysteinyl leukotrienes in virus-induced wheezing. *J. Allergy Clin. Immunol.* **103**, 630–636 (1999).
79. R. J. Lee, J. M. Kofonow, P. L. Rosen, A. P. Siebert, B. Chen, L. Doghramji, G. Xiong, N. D. Adappa, J. N. Palmer, D. W. Kennedy, J. L. Kreindler, R. F. Margolskee, N. A. Cohen, Bitter and sweet taste receptors regulate human upper respiratory innate immunity. *J. Clin. Invest.* **124**, 1393–1405 (2014).
80. K. Oymar, T. Halvorsen, L. Aksnes, Mast cell activation and leukotriene secretion in wheezing infants. Relation to respiratory syncytial virus and outcome. *Pediatr. Allergy Immunol.* **17**, 37–42 (2006).
81. M. Idzko, D. Ferrari, H. K. Eltzschig, Nucleotide signalling during inflammation. *Nature* **509**, 310–317 (2014).
82. M. Idzko, H. Hammad, M. van Nimwegen, M. Kool, M. A. M. Willart, F. Muskens, H. C. Hoogsteden, W. Luttmann, D. Ferrari, F. D. Virgilio, J. C. . Virchow Jr., B. N. Lambrecht, Extracellular ATP triggers and maintains asthmatic airway inflammation by activating dendritic cells. *Nat. Med.* **13**, 913–919 (2007).
83. J. Beale, A. Jayaraman, D. J. Jackson, J. D. R. Macintyre, M. R. Edwards, R. P. Walton, J. Zhu, Y. M. Ching, B. Shamji, M. Edwards, J. Westwick, D. J. Cousins, Y. Y. Hwang, A. M. Kenzie, S. L. Johnston, N. W. Bartlett, Rhinovirus-induced IL-25 in asthma exacerbation drives type 2 immunity and allergic pulmonary inflammation. *Sci. Transl. Med.* **6**, 256ra134 (2014).
84. M. Tizzano, M. Cristofoletti, A. Sbarbati, T. E. Finger, Expression of taste receptors in solitary chemosensory cells of rodent airways. *BMC Pulm. Med.* **11**, 3 (2011).
85. N. N. Patel, V. Triantafillou, I. W. Maina, A. D. Workman, C. C. L. Tong, E. C. Kuan, P. Papagiannopoulos, J. V. Bosso, N. D. Adappa, J. N. Palmer, M. A. Kohanski, D. R. Herbert, N. A. Cohen, Fungal extracts stimulate solitary chemosensory cell expansion in noninvasive fungal rhinosinusitis. *Int. Forum Allergy Rhinol.* **9**, 730–737 (2019).
86. C. K. Rane, S. R. Jackson, C. F. Pastore, G. Zhao, A. I. Weiner, N. N. Patel, D. R. Herbert, N. A. Cohen, A. E. Vaughan, Development of solitary chemosensory cells in the distal lung after severe influenza injury. *Am. J. Phys. Lung Cell. Mol. Phys.* **316**, L1141–L1149 (2019).
87. T. E. Taylor-Clark, C. Nassenstein, B. J. Undem, Leukotriene D4 increases the excitability of capsaicin-sensitive nasal sensory nerves to electrical and chemical stimuli. *Br. J. Pharmacol.* **154**, 1359–1368 (2008).
88. J. Wang, M. Kollarik, F. Ru, H. Sun, B. M. Neil, X. Dong, G. Stephens, S. Korolevich, P. Brohawn, R. Kolbeck, B. Undem, Distinct and common expression of receptors for inflammatory mediators in vagal nodose versus jugular capsaicin-sensitive/ TRPV1-positive neurons detected by low input RNA sequencing. *PLOS ONE* **12**, e0185985 (2017).
89. I. M. Chiu, L. B. Barrett, E. K. Williams, D. E. Strochlic, S. Lee, A. D. Weyer, S. Lou, G. S. Bryman, D. P. Roberson, N. Ghasemlou, C. Piccoli, E. Ahat, V. Wang, E. J. Cobos, C. L. Stucky, Q. Ma, S. D. Liberles, C. J. Woolf, Transcriptional profiling at whole population and single cell levels reveals somatosensory neuron molecular diversity. *eLife* **3**, e04660 (2014).
90. D. M. Lopes, F. Denk, S. B. McMahon, The molecular fingerprint of dorsal root and trigeminal ganglion neurons. *Front. Mol. Neurosci.* **10**, 304 (2017).
91. H. J. Solinski, M. C. Kriegbaum, P.-Y. Tseng, T. W. Earnest, X. Gu, A. Barik, A. T. Chesler, M. A. Hoon, Nppb Neurons Are Sensors of Mast Cell-Induced Itch. *Cell Rep.* **26**, 3561–3573.e4 (2019).

92. Y. Kanaoka, A. Maekawa, J. F. Penrose, K. F. Austen, B. K. Lam, Attenuated zymosan-induced peritoneal vascular permeability and IgE-dependent passive cutaneous anaphylaxis in mice lacking leukotriene C4 synthase. *J. Biol. Chem.* **276**, 22608–22613 (2001).
93. I. Matsumoto, M. Ohmoto, M. Narukawa, Y. Yoshihara, K. Abe, Skn-1a (Pou2f3) specifies taste receptor cell lineage. *Nat. Neurosci.* **14**, 685–687 (2011).
94. L. Homolya, W. C. Watt, E. R. Lazarowski, B. H. Koller, R. C. Boucher, Nucleotide-regulated calcium signaling in lung fibroblasts and epithelial cells from normal and $P2Y_2$ receptor (−/−) mice. *J. Biol. Chem.* **274**, 26454–26460 (1999).
95. Y. You, E. J. Richer, T. Huang, S. L. Brody, Growth and differentiation of mouse tracheal epithelial cells: Selection of a proliferative population. *Am. J. Phys. Lung Cell. Mol. Phys.* **283**, L1315–L1321 (2002).
96. M. G. Thomas, R. M. Marwood, A. E. Parsons, R. B. Parsons, The effect of foetal bovine serum supplementation upon the lactate dehydrogenase cytotoxicity assay: Important considerations for in vitro toxicity analysis. *Toxicol. in Vitro* **30**, 300–308 (2015).
97. N. A. Barrett, O. M. Rahman, J. M. Fernandez, M. W. Parsons, W. Xing, K. F. Austen, Y. Kanaoka, Dectin-2 mediates Th2 immunity through the generation of cysteinyl leukotrienes. *J. Exp. Med.* **208**, 593–604 (2011).
98. A. Dobin, C. A. Davis, F. Schlesinger, J. Drenkow, C. Zaleski, S. Jha, P. Batut, M. Chaisson, T. R. Gingeras, STAR: Ultrafast universal RNA-seq aligner. *Bioinformatics* **29**, 15–21 (2013).
99. D. S. DeLuca, J. Z. Levin, A. Sivachenko, T. Fennell, M.-D. Nazaire, C. Williams, M. Reich, W. Winckler, G. Getz, RNA-SeQC: RNA-seq metrics for quality control and process optimization. *Bioinformatics* **28**, 1530–1532 (2012).
100. Y. Liao, G. K. Smyth, W. Shi, The Subread aligner: Fast, accurate and scalable read mapping by seed-and-vote. *Nucleic Acids Res.* **41**, e108 (2013).
101. M. I. Love, W. Huber, S. Anders, Moderated estimation of fold change and dispersion for RNA-seq data with DESeq2. *Genome Biol.* **15**, 550 (2014).

Acknowledgments: We thank A. Chicoine (Brigham and Women's Hospital Human Immunology Center Flow Core) for help with FACS sorting. **Funding:** This work was supported by NIH grants R01 HL120952 and R01 AI134989 (to N.A.B.), U19 AI095219 (to N.A.B., Y.K., and L.G.B.), R01 HD098363 (to W.G.J.), R01 DC017503 (to I.M.), K08 AI132723 (to L.G.B.), the AAAAI/ALA Respiratory Disease Award (to N.A.B.), the AAAAI Foundation Faculty Development Award (to L.G.B.), the Steven and Judy Kaye Young Innovators Award (to N.A.B.), the Department of Defense Investigator-Initiated Research Award W81XWH-17-1-0527 (to Y.K. and N.A.B.), the Joycelyn C. Austen Fund for Career Development of Women Physician Scientists (to L.G.B.), and a donation by the Vinik family (to L.G.B.). **Author contributions:** Conceptualization: L.G.B. and N.A.B. Statistical analysis: L.G.B. and S.U. Investigation: L.G.B., S.U., N.H., Y.K., and N.A.B. Writing: L.G.B., N.A.B., S.U., I.M., and Y.K. Funding acquisition: N.A.B., L.G.B., I.M., W.G.J., and Y.K. Resources: Y.K., W.G.J., C.L., and I.M. **Competing interests:** The authors declare that they have no competing interests. **Data and materials availability:** The RNA sequencing data for this study have been deposited to the NCBI Gene Expression Omnibus and are accessible under accession number GSE139014. All other data needed to evaluate the conclusions in the paper are present in the paper or the Supplementary Materials. Skn-1a/Pou2f3 knockout mice are available from I.M. through a material transfer agreement with Monell Chemical Senses Center.

Submitted 21 April 2019
Accepted 19 December 2019
Published 17 January 2020
10.1126/sciimmunol.aax7224

Citation: S. Ualiyeva, N. Hallen, Y. Kanaoka, C. Ledderose, I. Matsumoto, W. G. Junger, N. A. Barrett, L. G. Bankova, Airway brush cells generate cysteinyl leukotrienes through the ATP sensor P2Y2. *Sci. Immunol.* **5**, eaax7224 (2020).